Journal of Molecular Structure 1358 (2026) 145287

Contents lists available at ScienceDirect

Journal of Molecular Structure

journal homepage: www.elsevier.com/locate/molstr

Novel piperazine–pyrimidine hybrids as potential anticancer agents against MCF-7 breast carcinoma: Synthesis, antimicrobial activity, antioxidant evaluation, and computational insights

Nabeel A. Abdul-Rida [a], Noor H. Youssef [a], Risala H. Allami [b], Yahia Bekker [c], Lanez Elhafnaoui [c], Najim A. Al-Masoudi [d,e,*]

[a] Department of Chemistry, College of Science, University of Qadisiyah, Diwanyiah, Iraq
[b] Department of molecular and medical biotechnology, College of Biotechnology, Al-Nahrain University, Jadriya, Baghdad, Iraq
[c] Laboratory of Valorisation and Technology of Saharian Resources (VTRS), Department of Chemistry, Faculty of Exact Sciences, University of El Oued, B.P.789, 39000, El Oued, Algeria
[d] Department of Chemistry, College of Science, University of Basrah, Basrah, Iraq
[e] Present address:78464 Konstanz, Germany

ARTICLE INFO

Keywords:
Anticancer activity
Antioxidant
Antifungal activity
Antibacterial activity
2-(Piperazin-1-yl)pyrimidine
In-silico computational studies

ABSTRACT

2-(Piperazin-1-yl)pyrimidine and its derivatives display a wide spectrum of biological activities, particularly demonstrating significant antimicrobial and anticancer properties. Here we report the one-step synthesis of 2-(2-(1-(4-aryl)ethylidene)hydrazinyl)-4-((4-(pyrimidin-2-yl)piperazin-1-yl)methylene)-4,5-dihydrothiazole derivatives **17–23**. All synthesized compounds were tested for antiproliferative activity against MCF-7 breast cancer cells, with compound **19** showing the highest potency (IC_{50} = 86.27 ug/mL, SI = 2.2). The total antioxidant capacity and antimicrobial activity of compounds **17–23** were also evaluated, with compound **21** demonstrating the strongest radical scavenging and antimicrobial effects. Molecular docking analyses revealed that compound **19** exhibited strong binding affinities toward estrogen receptor alpha (ERα) and epidermal growth factor receptor (EGFR) (−10.04 kcal.mol^{-1} for both targets), comparable to the reference drug tamoxifen (-10.61 for ERα and -7.92 for EGFR). ADMET profiling revealed that derivative **19** possesses a favorable pharmacokinetic and safety profile, characterized by high absorption, good solubility, and low predicted toxicity compared to tamoxifen. Furthermore, molecular dynamics simulations over 100 ns confirmed the structural stability, compactness, and sustained binding of compound **19** within the ERα and EGFR active sites. While these results suggest potential dual-target interactions, experimental studies are necessary to validate this activity.

1. Introduction

Pyrimidine-based compounds have exhibited considerable pharmacological potential, with the incorporation of piperazine into the pyrimidine scaffold represents a promising strategy for drug design and development [1–9]. Derivatives of 2-(piperazin-1-yl)pyrimidine have displayed diverse biological activities, including antimicrobial [10], anticancer [11], antioxidant [12], anti-inflammatory [13], and antimalarial [14] effects, underscoring their relevance in modern drug discovery. Ongoing research aims to optimize their chemical structures to enhance therapeutic efficacy while reducing adverse effects. Of particular note, 2-(piperazin-1-yl)pyrimidine itself functions as an antagonist of the α2-adrenergic receptor [15]. However, the azapirone class of compounds, including buspirone **1**, gepirone **2**, ipsapirone **3** (Fig. 1), tandospirone, and zalospirone possesses the pharmacologically active 1-(2-pyrimidinyl)piperazine (1-PP) moiety and are well recognized for their anxiolytic and antidepressant properties [16]. In addition, Al-Ghorbani et al. [17] synthesized a new series of (E)-1-(4-(4,6-diphenylpyrimidin-2-yl)piperazin-1-yl)-3-phenylprop-2-en-1-one derivatives and found that three compounds showed strong antiprotozoal activity against the NF54 chloroquine-sensitive strain of *Plasmodium falciparum* (IC_{50} = 0.18–0.21 μM), comparable to quinine and chloroquine. Several pyrimidine–piperazine derivatives have progressed to clinical use. Notably, imatinib (Fig. 1, 4), infigratinib, and dasatinib are marketed kinase inhibitors employed in cancer therapy. Among these, dasatinib (BMS-354,825) (Fig. 1, 5) [18,19] has been approved for the

* Corresponding author.
E-mail address: najim.al-masoudi@gmx.de (N.A. Al-Masoudi).

https://doi.org/10.1016/j.molstruc.2026.145287
Received 28 October 2025; Received in revised form 29 December 2025; Accepted 7 January 2026
Available online 9 January 2026

treatment of chronic myelogenous leukemia (CML) through inhibition of the BCR-ABL fusion gene [20], as well as for acute lymphoblastic leukemia (ALL), particularly in Philadelphia chromosome-positive (pH+) cases [21,22]. The BCR-ABL fusion gene arises from a reciprocal translocation between chromosomes 9 and 22, resulting in the production of a hyperactive tyrosine kinase protein that drives the development of CML [23]. Tokarski et al. [24] demonstrated that dasatinib's effectiveness against both wild-type and imatinib-resistant ABL mutants stems from its ability to bind multiple BCR-ABL conformations, underscoring the importance of kinase conformation in designing effective cancer inhibitors. Moreover, Nam et al. [25] reported that dasatinib exhibited therapeutic potential in metastatic prostate cancer driven by activated SFK and focal adhesion kinase signaling. Furthermore, Liu et al. [26] revealed that dasatinib markedly enhanced the sensitivity of P-gp-overexpressing MCF-7/Adr cells to doxorubicin in MTT assays, thereby increasing the cytotoxic effect of doxorubicin in these cells.

Building on the broad pharmacological significance of 2-(piperazine-1-yl)pyrimidine derivatives and our previous investigations of anticancer-active chemo-analogues [27–30], we report herein the rational design and one-pot synthesis of novel 2-(piperazine-1-yl)pyrimidine derivatives conjugated with substituted aryl-ethylidene-hydrazineyl-4,5-dihydrothiazole moieties. These compounds were evaluated for their antiproliferative effects against MCF-7 breast cancer cell line and their antioxidant properties. In addition, molecular docking, molecular dynamics simulations, and DFT analyses were carried out to gain deeper insights into their therapeutic potential.

2. Experimental

2.1. General information

Melting points were determined on a Gallenkamp SMP apparatus and are uncorrected. The IR spectra were recorded on FT-IR (Bruker Spectrophotometer), using KBr discs. ^{1}H and ^{13}C NMR spectra were recorded on Bruker AMX (400 MHz) (^{1}H) and 100 MHz (^{13}C) spectrometers, using DMSOd_6 solvent (chemical shifts δ in ppm). The reactions were monitored by thin layer chromatography, (eluent: hexane-EtOAc 4:1), and the spots were visualized using iodine vapor and UV light. Elemental (CHN) analyses were performed on a Thermo Scientific EA1112 elemental analyzer equipped with Eager 300 software. The elemental analysis results were measured and found to be within the acceptable range of ±0.3.

2.2. 1-Chloro-3-(4-(pyrimidin-2-yl)piperazin-1-yl)propane-2-one (8) [31]

Bis(chloromethyl) ketone (17.6 mg, 14.0 mmol) was dissolved in dry THF (15 mL) and placed in an ice bath. Subsequently, 2-(piperazin-1-yl) pyrimidine (**7**) (12.0 mmol) was added, followed by addition dropwise of Et_3N (1.9 mL, 13.2 mmol) dissolved in dry THF (50 mL). The reaction mixture was heated under reflux for 2.0 h. After completion of the reaction (monitored by TLC), the mixture was stirred at room temperature for 1 h. The precipitated product was filtered, washed with water, EtOH and dried. Yield 65 %, mp: 132–134 °C.

2.3. General method for the preparation of 2-(piperazin-1-yl)pyrimidine derivatives (17–23)

A mixture of **8** (240 mg, 1.0 mmol), thiosemicarbazide (91 mg, 1.0 mmol), 4-substituted acetophenones (1.0 mmol) and NaOAc (0.02 mmol) in EtOH (20 mL) was heated at 80 °C for 8 h. The reaction mixture was monitored by TLC. After completion, the reaction was cooled at room temperature and the precipitated product was filtered off and purified by recrystallization from EtOH to give the desired products in good yields.

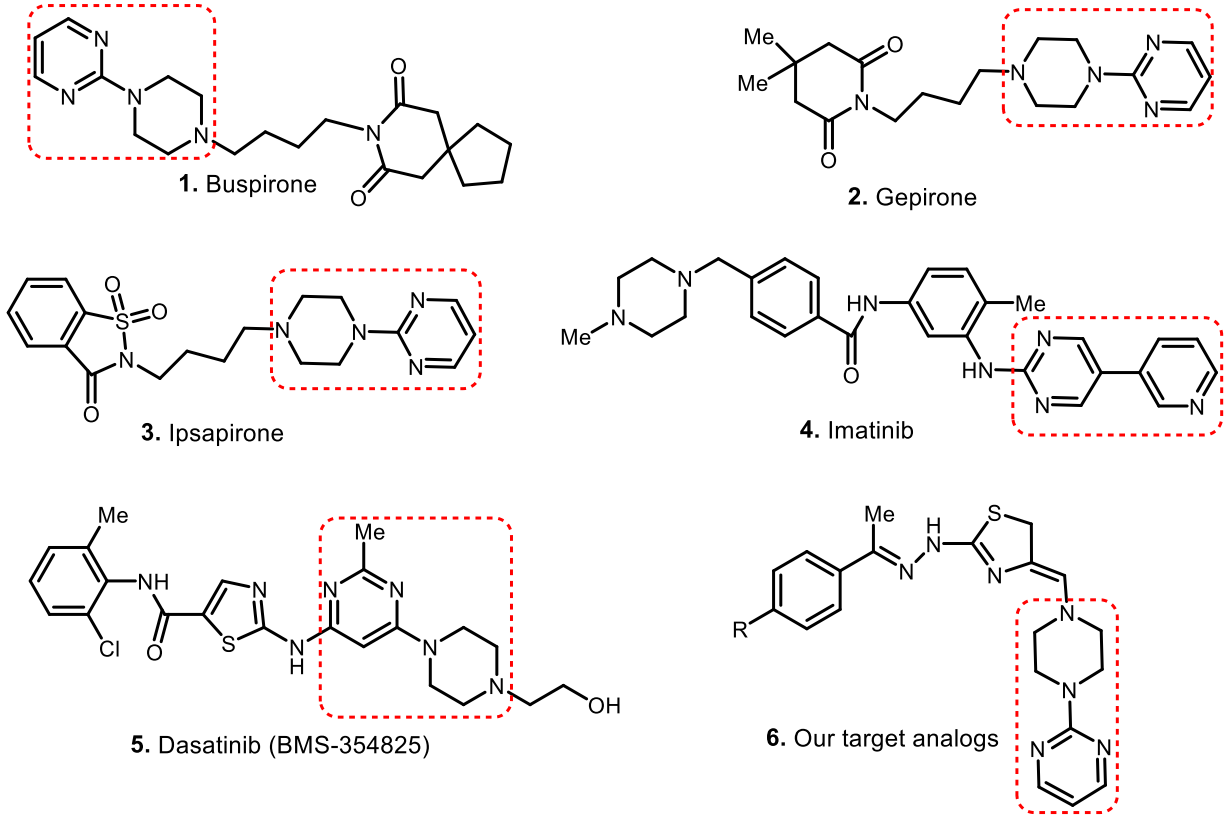

Fig. 1. Representative drugs featuring 2-(piperazin-1-yl)pyrimidine backbone and our target compounds.

2.3.1. 2-(2-(1-(4-Chlorophenyl)ethylidene)hydrazineyl)-4-((4-(pyrimidin-2-yl)piperazin-1-yl) methylene)-4,5-dihydrothiazole (17)

From 4-chloro-acetophenone (154 mg). Yield: 321 mg (75 %) as a yellow powder, mp: 130–132 °C, $R_f = 0.58$; IR (KBr): 3460 (NH) 3145, 3052 (Ar-*CH*), 1716 (*C* = *N*), 1588 (*C* = *C*), 831 (C—Cl), ^{1}H NMR (400 MHz, DMSO-d_6): δ 10.24 (s, 1H, NH), 8.42–8.29 (m, 2H, $H_{pyrimidine}$), 7.96 (dd, 2H, *J* = 7.5 Hz, $H_{arom.}$−1 + $H_{arom.}$−6), 7.56 (dd, 2H, *J* = 7.5 Hz, $H_{arom.}$−2 + $H_{arom.}$−5), 6.95 (br s., 2H, *C* = $C_{17}H$ + $H_{pyrimidine}$-5), 3.42 (s, 2H, $CH2_{thiazole}$-5), 3.21 (m, 8H, $H_{piperazine}$), 2.27 (s, 3H, Me). ^{13}C NMR (100 MHz, DMSO-d_6) δ 160.7 ($C_{pyrimidine}$-2), 158.0 ($C_{pyrimidine}$-4 + $C_{pyrimidine}$-6), 154.5 ($C_{thiazole}$-2), 146.5 (Me-*C* = *N*), 136.4 (C—Cl + $C_{arom.}$−6), 133.8 (*C*═*CH*-piperazine), 128.3, 128.1 ($C_{arom.}$−1 + $C_{arom.}$−5), 111.1 ($C_{pyrimidine}$-5 + $C_{thiazole}$-4), 45.3, 42.2 (4x$C_{piperazine}$) 13.7 ($C_{thiazole}$-5), 10.3 (Me). Elemental analysis calcd for $C_{20}H_{22}ClN_7S$ (427.13): C 56.13; H, 5.18; N, 22.91. Found: C, 55.94; H, 5.02, N, 22.69.

2.3.2. 4-(1-(2-(4-((4-(Pyrimidin-2-yl)piperazin-1-yl)methylene)-4,5-dihydrothiazol-2-yl) hydrazineylidene)ethyl)phenol (18)

From 4-hydroxy-acetophenone (136 mg). Yield: 319 mg (78 %) as a brown powder, mp: 122–124 °C, $R_f = 0.64$; IR (KBr): 3474 (NH) 3363 (OH), 3167 (Ar-*CH*), 1690 (*C* = *N*), 1596 (*C* = *C*), 829 (C—Cl), ^{1}H NMR (400 MHz, DMSO-d_6): δ 9.86 (s, 1H, NH), 8.14 (s, 1H, OH), 7.81–7.79 (m, 2H, $H_{pyrimidine}$), 7.74 (dd, 2H, *J* = 7.3 Hz, $H_{arom.}$−1 + $H_{arom.}$−5), 6.87 (d, 1H, $J_{4,5} = J_{5,6} = 5.1$ Hz, $H_{pyrimidine}$-5), 6.77 (m, 3H, $H_{arom.}$−2 + $H_{arom.}$-4 + *C* = $C_{17}H$), 3.37 (s, 2H, $CH2_{thiazole}$-5), 3.11 (m, 2H, $H_{piperazine}$), 3.03 (m, 2H, $H_{piperazine}$), 2.23 (s, 3H, Me). ^{13}C NMR (100 MHz, DMSO-d_6) δ 162.1 ($C_{pyrimidine}$-2 + *C*—OH), 158.0 ($C_{pyrimidine}$-4 + $C_{pyrimidine}$-6), 150.1 ($C_{thiazole}$-2), 148.3 (Me-*C* = *N*), 130.0 (*C*═*CH*-piperazine), 128.3, 128.0 ($C_{arom.}$−2 + $C_{arom.}$−4, 115.1 ($C_{arom.}$−1 + $C_{arom.}$−5), 114.9 ($C_{thiazole}$-4 + $C_{pyrimidine}$-5), 45.3, 45.2 (4x$C_{piperazine}$), 13.7 ($C_{thiazole}$-5 + Me). Elemental analysis calcd for $C_{20}H_{23}N_7OS$ (409.17): C 58.66; H, 5.66; N, 23.94. Found: C, 58.41; H, 5.53, N, 23.73.

2.3.3. 2-(2-(1-(4-Bromophenyl)ethylidene)hydrazineyl)-4-((4-(pyrimidin-2-yl)piperazin-1-yl) methylene)-4,5-dihydrothiazole (19)

From 4-bromo-acetophenone (198 mg). Yield: 377 mg (80 %) as a light yellow powder, $R_f = 0.50$; mp: 128–130 °C IR (KBr): 3432 (NH) 3263, 3158 (Ar-*CH*), 1700 (*C* = *N*), 1602 (*C* = *C*), 846 (C—Cl), ^{1}H NMR (400 MHz, *DMSO-d*$_6$): δ 10.24 (s, 1H, NH), 8.29–7.98 (m, 2H, $H_{pyrimidine}$), 7.88 (dd, 2H, *J* = 7.4 Hz, $H_{arom.}$−2 + $H_{arom.}$−4), 7.54 (dd, 2H, *J* = 7.4 Hz, $H_{arom.}$−1 + $H_{arom.}$−5), 6.46 (br s., 2H, *C* = $C_{17}H$ + $H_{pyrimidine}$-5), 3.35–3.03 (m, 10H, $H_{piperazine}$ + $CH2_{thiazole}$-5), 2.27 (s, 3H, Me). ^{13}C NMR (100 MHz, DMSO-d_6) δ 169.9 ($C_{pyrimidine}$-2), 157.4 ($C_{pyrimidine}$-4 + $C_{pyrimidine}$-6), 153.8 ($C_{thiazole}$-2), 142.7 (Me-*C* = *N*), 137.4 ($C_{arom.}$−6), 132.3 ($C_{arom.}$−2 + $C_{arom.}$−4), 130.1 (*C*═*CH*-piperazine), 129.4, 128.8 ($C_{arom.}$−1 + $C_{arom.}$−5), 115.2 ($C_{pyrimidine}$-5 + $C_{thiazole}$-4), 50.2, 46.2 (4x$C_{piperazine}$), 24.9 ($C_{thiazole}$-5), 19.0 (Me). Elemental analysis calcd for $C_{20}H_{22}BrN_7S$ (471.08): C 50.85; H, 4.69; N, 20.76. Found: C, 50.62; H, 4.53, N, 20.49.

2.3.4. 2-(2-(1-(4-Nitrophenyl)ethylidene)hydrazineyl)-4-((4-(pyrimidin-2-yl)piperazin-1-yl) methylene)-4,5-dihydrothiazole (20)

From 4-nitro-acetophenone (165 mg). Yield: 319 mg (74 %), a light-yellow powder, mp: 133–136 °C, $R_f = 0.61$; IR (KBr): 3235 (NH) 3108, 3070 (Ar-*CH*), 1672 (*C* = *N*), 1595 (*C* = *C*), 847 (C—Cl), ^{1}H NMR (400 MHz, DMSO-d_6): δ 10.44 (s, 1H, NH), 8.44–8.14 (m, 6H, $H_{arom.}$ + $H_{pyrimidine}$ 4 + $H_{pyrimidine}$ 6), 6.71 (br s., 2H, *C* = $C_{17}H$ + $H_{pyrimidine}$-5), 3.50 (s, 2H, $CH2_{thiazole}$-5), 3.41–3.00 (m, 4H, $H_{piperazine}$), 2.34 (s, 3H, Me). ^{13}C NMR (100 MHz, DMSO-d_6) δ 167.9 ($C_{pyrimidine}$-2), 156.6 ($C_{thiazole}$-2), 153.9 ($C_{pyrimidine}$-4 + $C_{pyrimidine}$-6 + *C*—NO_2), 148.2 (Me-*C* = *N*), 138.5–121.3 ($C_{arom.}$ + *C* = *C*-piperazine), 115.9 ($C_{arom.}$), 115.9 ($C_{thiazole}$-4), 115.6 ($C_{pyrimidine}$-5), 45.7, 43.0 (4x$C_{piperazine}$), 22.4 ($C_{thiazole}$-5), 14.9 (Me). Elemental analysis calcd for $C_{20}H_{22}N_8O_2S$ (438.16): C 54.78; H, 5.06; N, 25.55. Found: C, 54.55; H, 4.96, N, 25.38.

2.3.5. 4-(1-(2-(4-((4-(Pyrimidin-2-yl)piperazin-1-yl)methylene)-4,5-dihydrothiazol-2-yl) hydrazineylidene)ethyl)aniline (21)

From 4-amino-acetophenone (165 mg). Yield: mg (78 %) as a yellow powder, mp: 170–172 °C, $R_f = 0.73$; IR (KBr): 3373, 3310 (NH), 3209 (Ar-*CH*), 1665 (*C* = *N*), 1603 (*C* = *C*), 828 (C—Cl), ^{1}H NMR (400 MHz, DMSO-d_6): δ 9.93 (s, 1H, NH), 8.06 (br s., 2H, $H_{pyrimidine}$ 4 + $H_{pyrimidine}$ 6), 7.64 (dd, 2H, *J* = 7.5 Hz, $H_{arom.}$−2 + $H_{arom.}$−5), 6.56–6.04 (m, 4H, $H_{arom.}$−3 + $H_{arom.}$-5 + *C* = $C_{17}H$ + $H_{pyrimidine}$-5), 5.46 (br s., 2H, NH_2), 3.60 (s, 2H, $CH2_{thiazole}$-5), 3.50 (m, 8H, $H_{piperazine}$), 2.36 (s, 3H, Me). ^{13}C NMR (100 MHz, DMSO-d_6) δ 164.4 ($C_{pyrimidine}$-2), 157.6 154.0 ($C_{pyrimidine}$-4 + $C_{pyrimidine}$-6), 154.0 ($C_{thiazole}$-2), 150.1 (C—NH_2), 148.9 (Me-*C* = *N*), 130.4 (*C*═*CH*-piperazine), 127.8 ($C_{arom.}$−1 + $C_{arom.}$−5 + $C_{arom.}$−6), 113.1 ($C_{arom.}$−2 + $C_{arom.}$−4 + $C_{thiazole}$-4), 112.4 ($C_{pyrimidine}$-5), 55.9, 45.6 (4x$C_{piperazine}$), 13.4 ($C_{thiazole}$-5 + Me). Elemental analysis calcd for $C_{20}H_{24}N_8S$ (408.18): C 58.80; H, 5.92; N, 27.43. Found: C, 58.61; H, 5.88, N, 27.25.

2.3.6. 2-(2-(1-(4-Methoxyphenyl)ethylidene)hydrazinyl)-4-((4-pyrimidin-2-yl)piperazin-1-yl)methylene)-4,5-dihydrothiazole (22)

From 4-methoxy-acetophenone (mg). Yield: mg (83 %) a brown powder, mp: 115–118 °C, $R_f = 0.59$; IR (KBr): 3423 (NH), 3149, 3001 (Ar-*CH*), 1715 (*C* = *N*), 1587 (*C* = *C*), 813 (C—Cl), ^{1}H NMR (400 MHz, DMSO-d_6): δ 10.20 (s, 1H, NH), 8.26 (br s., 2H, $H_{pyrimidine}$ 4 + $H_{pyrimidine}$ 6), 7.91 (br s., $H_{arom.}$−2 + $H_{arom.}$−6), 7.36 (br s., 2H, $H_{arom.}$−3 + $H_{arom.}$−5), 6.19 (*C* = $C_{17}H$ + $H_{pyrimidine}$-5), 3.83(s, 5H, OMe + $CH2_{thiazole}$-5), 2.95–2.92 (m, 8H, $H_{piperazine}$), 2.29 (s, 3H, Me). ^{13}C NMR (100 MHz, DMSO-d_6) δ 166.7 ($C_{pyrimidine}$-2), 155.0 ($C_{thiazole}$-2 + $C_{pyrimidine}$-4 + $C_{pyrimidine}$-6), 150.6 (*C*—OMe), 143.0 (Me-*C* = *N*), 130.8 (*C*═*CH*-piperazine), 130.3 ($C_{arom.}$−6), 126.6 ($C_{arom.}$−1 + $C_{arom.}$−5), 120.9 ($C_{pyrimidine}$-5), 116.9 ($C_{thiazole}$-4 + $C_{arom.}$−2 + $C_{arom.}$−4), 62.9 (OMe), 52.2 (4x$C_{piperazine}$), 21.4 ($C_{thiazole}$-5), 20.4 (Me). Elemental analysis calcd for $C_{21}H_{25}N_7OS$ (423.54): C 59.55; H, 5.95; N, 23.15. Found: C, 59.38; H, 5.86, N, 22.97.

2.3.7. 2-(2-(1-Phenylethylidene)hydrazineyl)-4-((4-pyrimiden-2-yl) piperazin-1-yl)methylene)-4,5-dihydrothiazole (23)

From acetophenone (mg). Yield: mg (83 %), a light brown bowder, mp: 142–144 °C, $R_f = 0.78$;

IR (KBr): 3441 (NH), 3034, 3006 (Ar-*CH*), 1736 (*C* = *N*), 1645 (*C* = *C*), 808 (C—Cl), ^{1}H NMR (400 MHz, DMSO-d_6): δ 10.20 (s, 1H, NH), 8.41 (br s., 2H, $H_{pyrimidine}$ 4 + $H_{pyrimidine}$ 6), 7.92–7.82 (m., $H_{arom.}$−1 + $H_{arom.}$−5), 7.45–7.35 (m, 3H, $H_{arom.}$−2 + + $H_{arom.}$−3 + $H_{arom.}$−4), 6.72 (*C* = $C_{17}H$ + $H_{pyrimidine}$-5), 3.86 (s, 2H, $CH2_{thiazole}$-5), 3.10–3.00 (m, 8H, $H_{piperazine}$), 2.36 (s, 3H, Me). ^{13}C NMR (100 MHz, DMSO-d_6) δ 160.7 ($C_{pyrimidine}$-2), 158.0 ($C_{thiazole}$-2 + $C_{pyrimidine}$-4 + $C_{pyrimidine}$-6), 147.8 (Me-*C* = *N*), 137.7 ($C_{arom.}$−6), 129.6, 129.1, 128.3, 126.5, 126.4, 126.3 (*C*═*CH*-piperazine + $C_{arom.}$), 111.0 ($C_{pyrimidine}$-5 + $C_{thiazole}$-4), 45.2 (4x$C_{piperazine}$), 13.9 ($C_{thiazole}$-5 + Me). Elemental analysis calcd for $C_{20}H_{23}N_7OS$ (393.17): C 61.04; H, 5.89; N, 24.92. Found: C, 60.88; H, 5.76, N, 24.79.

2.4. Biological assays

2.4.1. In vitro anticancer activity

2.4.1.1. Cancer cell lines. The MCF-7 human breast adenocarcinoma cell line (HTB-22™) was obtained from the American Type Culture Collection (ATCC, Rockville, MD, USA). Cells were grown in DMEM and maintained in RPMI-1640 medium, both supplemented with 10 % heat-inactivated fetal bovine serum (FBS), 1 % (v/v) penicillin (10,000 U/mL)–streptomycin (10 mg/mL), and 1 % (v/v) L-glutamine (200 mM) (all from Sigma-Aldrich). Cultures were maintained at 37 °C in a humidified atmosphere with 5 % CO_2.

2.4.1.1. Proliferation assay. To evaluate cytotoxicity, an MTT cell

viability assay [32] was performed in 96-well plates. MCF-7 cells were seeded at a density of 1 × 10^4 cells/well. After reaching a confluent monolayer (typically within 24 h), cells were treated with the test compound at a final concentration of 1000 ug/mL. Following 72 h of exposure, the culture medium was removed, and 28 uL of MTT solution (2 mg/mL) was added to each well. Plates were incubated for 2 h at 37 °C, after which the MTT solution was discarded. The resulting formazan crystals were solubilized by adding 100 uL of dimethyl sulfoxide (DMSO) and incubating at 37 °C for 15 min with gentle shaking. Absorbance was measured at 620 nm using a microplate reader. All experiments were carried out in triplicate.

The inhibition rate (IR) of cell growth was calculated according to the following equations:

$$\text{Proliferationrate } (PR) = B/A * 100 \quad (1)$$

where A is the mean optical density of untreated wells and B is the optical density of treated wells, and the inhibition rate (IR) is calculated as: *(IR) = 100- PR.*

2.4.2. Total antioxidant capacity by phosphomolybdate assay

The total antioxidant activity (TAC) of the fractions was evaluated using the phosphomolybdate method described by Prieto et al. [33], with ascorbic acid serving as the reference standard. Briefly, 1.0 mL of each sample solution was combined with 1.0 mL of the reagent solution containing 0.6 M sulfuric acid, 28 mM sodium phosphate, and 4 mM ammonium molybdate. The mixtures were capped and incubated in a water bath at 95 °C for 90 min. After cooling to room temperature, absorbance was measured at 695 nm using a UV-2450 spectrophotometer (Shimadzu, Japan). A blank was prepared by mixing 1.0 mL of the reagent solution with an equal volume of solvent under the same conditions.

All experiments were performed in duplicate. The antioxidant capacity (%) was calculated using the equation:

$$\text{Totalantioxidantcapacity } \% = \left[(A_{\text{control}}) - A_{\text{sample}}\right) / (C_{\text{ontrol}})] \times 100$$

2.4.3. Antifungal and antibacterial activity

The antimicrobial activity of the test compounds was evaluated against the bacterial strain *Escherichia coli*(ATCC 25,922) and the yeast fungal strain *Candida albicans* using the well diffusion method [34]. For the antibacterial activity evaluation, a stock solution of the synthesized compounds was prepared at a concentration of 100 mg/mL by dissolving them in dimethyl sulfoxide (DMSO). Bacterial isolate (*E.coli*(ATCC 25, 922) was cultured on Mueller Hinton agar plates by spreading a suspension standardized to 10^8 CFU/mL (corresponding to a 0.5 McFarland standard). Wells with a diameter of 6 mm were created using a sterile cork borer, and 50 uL of each test compound was gently added to the wells. The plates were incubated at 37 °C for 24 h, after which the mean inhibition zone (IZ) diameters, measured in millimeters (mm), were determined in triplicate.

The antifungal activity of all the title compounds was primary screened in vitro using the well diffusion method as described previously on PDA plates. Fungal isolate (*C. albicans*) was subcultured on sterile PDA plates and incubated at 37 °C for 72 hr. After fungal spore suspensions were prepared at 1 × 10^6 cell /mL, a 150 mL was vaccinated on fresh PDA plates by spreading using a sterile L-shape. Following making four holes 6 mm in diameter per a plate by a sterile cork borer, then were flooded by 50 mL of compounds stock solutions with three replicates each. The plates were incubated at 37 °C for 72 h. The inhibitory activity of tested compounds against fungal growth was observed by measured the inhibition zone diameter in mm. All experiments were carried out in triplicate.

2.5. In silico studies

2.5.2. Molecular docking

Molecular docking simulations were carried out using AutoDock Tools (ADT) version 1.5.7 [35], applying the Lamarckian Genetic Algorithm (LGA) for conformational sampling and binding optimization. The synthesized 2-(piperazin-1-yl)pyrimidine compounds **17–23** were energy-minimized using the MMFF94 force field implemented in Avogadro 1.2.0 [36]. The 3D structure of the reference anticancer agent tamoxifen (TMX) was retrieved from the PubChem database [37] The crystal structures of human estrogen receptor alpha (ERα, PDB ID: 1ERR) and epidermal growth factor receptor tyrosine kinase (EGFR, PDB ID: 3W2S) were retrieved from the Protein Data Bank [38]. All co-crystallized ligands, ions, and water molecules were removed. Polar hydrogens were added, Kollman charges were assigned, and the structures were saved in PDBQT format for docking [39–43]. Ligands were assigned flexible torsions, while the receptors were kept rigid.

Docking grids were defined around the respective active sites, with dimensions of 50 × 40 × 42 Å for ERα and 42 × 30 × 44 Å for EGFR. The grid centers were set at ($X = 67.930$, $Y = 34.785$, $Z = 74.193$) for ERα and ($X = 4.931$, $Y = 1.214$, $Z = 10.249$) for EGFR. Docking results were ranked according to their binding free energies (ΔG, kcal/mol), and the most favorable conformations (lowest energy poses) were selected for further interaction analysis [43].

Docked complexes were visualized using Discovery Studio Visualizer 2021 to identify hydrogen bonds, and hydrophobic interactions [44]. To validate the reliability of the docking protocol, redocking was performed by reintroducing the native co-crystallized ligand into the active site of each receptor. The docking method was considered valid when the root-mean-square deviation (RMSD) between the predicted and experimental poses was below 2.0 Å [41,42] .

2.5.3. ADMET study

The absorption, distribution, metabolism, excretion, and toxicity (ADMET) properties of the synthesized compounds **17–23** were evaluated to assess their drug-likeness and safety profiles. The SwissADME and pkCSM web server [45,46] was used to predict physicochemical parameters, Lipinski's rule of five, water solubility, lipophilicity (LogP), and gastrointestinal (GI) absorption. Additionally, pharmacokinetic properties such as blood–brain barrier (BBB) permeability, P-glycoprotein (P-gp) substrate prediction, and cytochrome P450 (CYP) enzyme interactions were analyzed. Toxicological assessment was conducted using the ProTox-II server [47], which estimated the toxicity class, median lethal dose (LD_{50}) in rats, and potential organ-specific toxicities, including hepatotoxicity, cytotoxicity, and carcinogenicity.

2.5.4. Molecular dynamics simulation

Molecular dynamics simulations (MDS) were performed to investigate the stability and conformational dynamics of the ERα and EGFR complexes with their respective ligands. All simulations were conducted using the GROMACS 2024.4 software package for a total simulation time of 100 ns [48]. Ligand topology and parameter files were generated using the SwissParam web server [49], which provided the structural parameters required for accurate molecular modeling [40]. The receptor topologies were prepared using the CHARMM36 all-atom force field, ensuring an accurate and detailed description of protein–ligand interactions throughout the simulation [50]. Each protein–ligand complex was placed in a cubic simulation box and solvated using the TIP3P water model. To maintain charge neutrality and mimic physiological conditions, appropriate numbers of Na^+ and Cl^- counterions were added [39]. Energy minimization of each solvated and neutralized system was performed using the steepest descent algorithm until the maximum force acting on the system was below 10.0 kJ/mol ensuring structural stability prior to equilibration [40].

The systems were equilibrated in two stages. The first stage involved constant-volume, constant-temperature (NVT) equilibration for 100 ps

at 300 K using a velocity-rescaling thermostat with a coupling constant of 0.1 ps. The second stage employed constant-pressure, constant-temperature (NPT) equilibration for an additional 100 ps using the Berendsen barostat with a pressure coupling constant of 2.0 ps [41]. Subsequently, a 100-ns production run was performed to examine the dynamic behavior and stability of each receptor–ligand complex. Structural and dynamic properties were analyzed to assess system behavior over time: root-mean-square deviation (RMSD) was computed to evaluate overall structural stability; root-mean-square fluctuation (RMSF) assessed residue-level flexibility; the radius of gyration (Rg) quantified protein compactness; and the solvent-accessible surface area (SASA) measured the degree of solvent exposure of the protein surface.

3. Results and discussion

3.1. Chemistry

The target compounds, 2-(2-(1-(4-aryl)ethylidene)hydrazinyl)-4-((4-(pyrimidin-2-yl)piperazin-1-yl)methylene)-4,5-dihydrothiazole derivatives **17–23** were synthesized *via* a two-step sequence. First, 1-chloro-3-(4-(pyrimidin-2-yl)piperazin-1-yl)propan-2-one (**8**) was prepared from 2-(piperazin-1-yl)pyrimidine (**7**) by reaction with 1,3-dichloropropan-2-one in the presence of Et_3N in dry THF, affording compound **8** in 73 % yield [31]. Subsequently, compound **8** was reacted with thiosemicarbazide (**9**) and a series of 4-substituted acetophenones, namely 4-chloro, 4-hydroxy, 4-bromo, 4-nitro, 4-amino, 4-methoxy, and unsubstituted acetophenone (**10–16**) in the presence of NaOAc in EtOH to afford the corresponding 4-(aryl)ethylidenehydrazinyl-thiazole analogs **17–23** in 74–83 % yields (Scheme 1).

The proposed mechanism for the formation of compounds **17–23** through a one-pot, three-component reaction involving 4-substituted acetophenones **10–16**, thiosemicarbazide (**9**), and 1-chloro-3-(4-(pyrimidin-2-yl)piperazin-1-yl)propan-2-one (**8**), catalyzed by anhydrous sodium acetate, is illustrated in Scheme 2 [51].

The structures of the newly synthesized compounds were identified from their IR, ^1H, ^{13}C NMR spectra. The N—H stretching vibrations of the 2-(piperazin-1-yl)pyrimidine derivatives **17–23** appeared in the range υ 3235–3474 cm^{-1}. Medium to weak absorption bands were observed at 3006–3263 cm^{-1}, while bands in the 1587–1645 cm^{-1} region were attributed to vibrations characteristic of the aromatic ring and the ($C4_{thiazole}$=CH-piperazine) stretching. In addition, a strong absorption band in the range υ 1665–1736 cm^{-1} was assigned to $C = N$ stretching. In the ^1H NMR spectra, H-4 and H-6 of the pyrimidine backbone appeared as multiplets or broad singlets in the region δ 7.81–7.79 and δ 7.79–8.24 ppm, respectively. The doublets, multiplets, or broad singlets observed in the range δ 6.19–6.95 ppm were assigned to H-5 of the pyrimidine residue together with the olefinic protons ($C = C_{17}H$). The CH_2–5 proton of the thiazole moiety appeared as singlets in the range δ 3.37–3.86 ppm. The eight protons of the piperazine ring resonated as multiplets or broad singlets in the range δ 2.92–3.42 ppm. All aromatic and aliphatic protons were fully characterized (see Experimental section). In the ^{13}C NMR spectra of compounds **17–23**, the lower field resonances in the range δ 160.7–169.9 ppm corresponded to C-2 of the pyrimidine backbone, while those in the range δ 155.0–158.7 ppm and 111.0–120.9 ppm, were assigned to C-4 + *C*-6 and C-5 of the same ring, respectively. Furthermore, C-2 of the thiazole moiety were observed in the range δ 150.1–158.0 ppm, whereas C-4 and C-5 of the same ring appeared in the range δ 111.0–116.9 and 13.7–21.4 ppm, respectively. Resonances in the range δ 142.7–148.9 ppm were attributed to the carbon atoms of the Me-$C = N$ group, while the signals in the range δ 42.2–55.9 ppm were assigned to the piperazine carbon atoms. The other aromatic and aliphatic carbon atoms were fully analyzed (see Experimental section). The gradient-selected HMBC spectrum [52] of **17** revealed $^3J_{C,H}$ coupling between the CH_2 protons of the thiazole moiety at δ_H 3.37 ppm and the carbon atom of *C*═*CH*-piperazine group at δ_C 130.0 ppm. Additionally, a $^3J_{C,H}$ coupling was observed between the same thiazole CH_2 protons and carbon C-2 of the thiazole ring at δ_C 150.1 ppm. A $^2J_{C,H}$ coupling was noted between proton of the *C*═*CH*-piperazine group at δ_H 6.95 ppm and C-4 of the thiazole residue at δ_C 111.1 ppm. Furthermore, a $^3J_{C,H}$ coupling was identified between H-1 and H-5 of the aromatic ring at δ_H 7.74 ppm and the carbon atom of the Me-$C = N$ group at δ_C 148.3 ppm (Fig. 2).

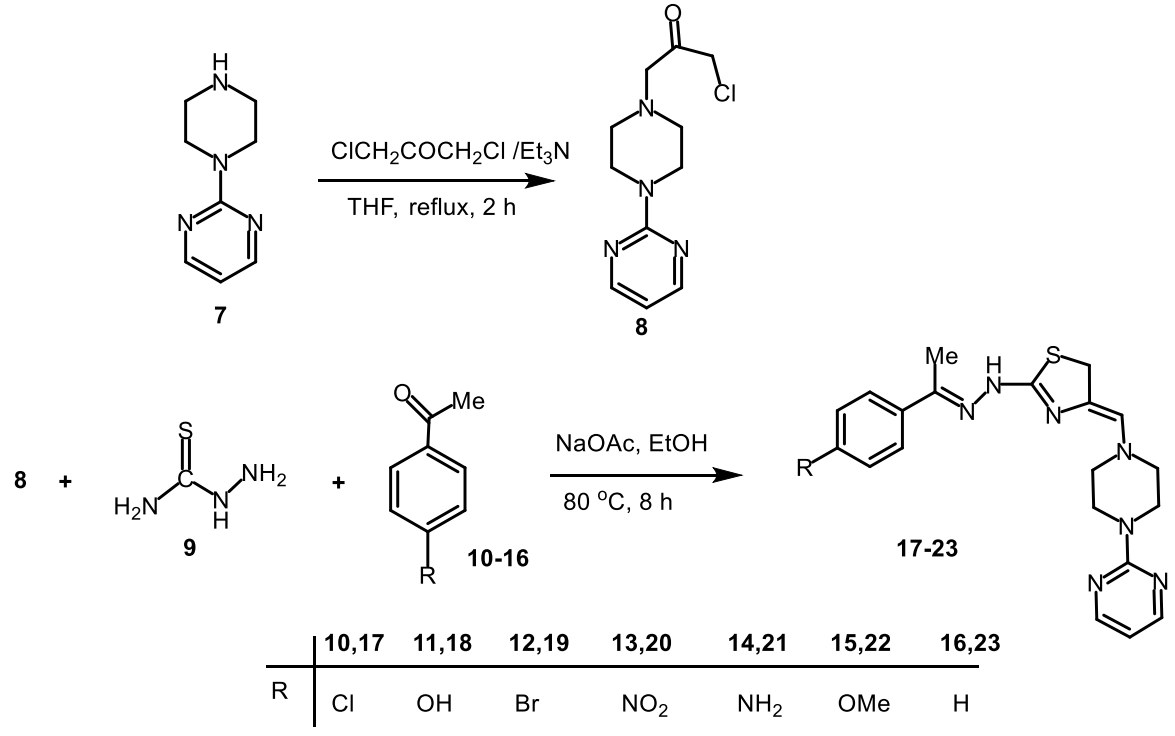

Scheme 1. Synthesis of 2-(piperazin-1-yl)pyrimidine-thiazole derivatives **17–23.**

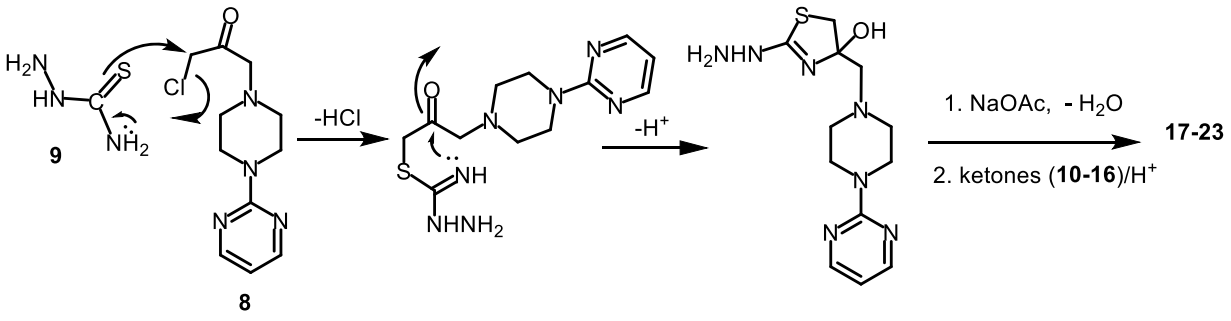

Scheme 2. Proposed mechanism for the formation of 4,5-dihydrothiazole derivatives **17–23**.

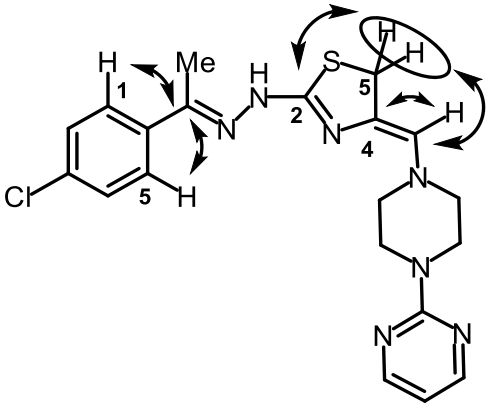

Fig. 2. $J_{C,H}$ correlations in the HMBC NMR spectrum of **17**.

3.2. Biological evaluation

3.2.1. Anticancer activity against breast cancer (MCF-7)

The cytotoxic activities of all newly synthesized compounds were evaluated against human breast adenocarcinoma (MCF-7) and primary neonatal human dermal fibroblast (HDFn) cell lines using the MTT assay [32], with tamoxifen (TMX) and taxol as reference drugs. IC_{50} values (ug/mL) were determined for each compound and are summarized in Table 1. The results indicated that substitution on the 2-(piperazin-1-yl) pyrimidine scaffold markedly affected cytotoxic activity. Several compounds demonstrated poor to moderate cytotoxicity toward the MCF-7 cell line. Among them, compound **19** displayed good activity, with an IC_{50} of 86.27 ug/mL compared to 186.7 ug/mL in healthy cells (HDFn), giving a selectivity index (SI) of 2.2. Compounds **20** and **21** also exhibited anticancer activity against the MCF-7 cell line, with IC_{50} values of 97.2 and 95.9 ug/mL, respectively. In contrast, the healthy HDFn cells showed IC_{50} values of 222.5 and 211.5 ug/mL, respectively, yielding SI values of 2.3 and 2.2, respectively.

Table 1
The anticancer activity of compounds **17–23**, tamoxifen and taxol.

Compd.	MCF (IC_{50}, ug/mL)	HdFn (IC_{50}, ug/mL)	SI*
17	91.6	196.1	2.1
18	118.1	226.1	1.9
19	86.27	86.27	2.2
	(183.2 uM)	(396.4 uM)	
20	97.2	222.5	2.3
21	95.9	211.5	2.2
22	96.0	181.4	1.2
23	131.1	155.4	1.2
TMX	75.67	162.9	2.2
Taxol	(203.7 uM)	(438.5 uM)	3.1
	57.9	176.6	
	(67.8 uM)	(206.8 uM)	

* SI: Selectivity index, TMX: Tamoxifen.

Regarding the structure–activity relationship, TuYuN et al. [53] have reported that the *para*-bromo-phenyl group is a crucial structural motif that can greatly enhance a compound's anticancer potency, as evidenced by studies on brominated plastoquinone and similar drug candidates. Furthermore, Geunin et al. [54] demonstrated that the inhibition of tumor cell proliferation in vitro is strongly influenced by both the type and position of halogen substituents on the phenyl ring. Their findings revealed that a *para*-bromo substituent significantly enhances the anticancer activity of 1-hydroxymethylene-1,1-bisphosphonic acids (HMBPs), with the potency trend (bromine > chlorine > fluorine) closely corresponding to the atomic volume of the substituent. Our current findings align with those of TuYuN, Geunin, and their research teams, showing that compound **19**, which contains a *para*-bromo substituent on the phenyl ring, exhibits superior antiproliferative activity compared to other analogues. However, Al-Salami et al. [55] demonstrated that introducing a hydrazinyl-4, 5-dihydrothiazole moiety into a compound is closely associated with significant anticancer activity, mainly through the induction of apoptosis, inhibition of kinases, disruption of the cell cycle, and potentially enhanced drug delivery via tumor-specific release mechanisms. Based on these observations, compound **19**, bearing the hydrazinyl-4, 5-dihydrothiazole group, is proposed to play a crucial role in inhibiting angiogenesis, a pivotal process in cancer progression. These structural features collectively act in synergy to effectively suppress tumor growth (Fig. 3). However, when considering the activity order of various substituents at para position of the phenyl group against MCF-7 cancer cell line, the ranking was as follows: 4-Br (most active) (**19**) > 4-Cl (**17**) > 4-NH_2 (**21**) > 4-OMe (**22**) > 4-NO_2 (**20**) > 4-OH (**18**) = *H* (**23**) (least active). Additionally, the selectivity index (SI) is essential in anticancer drug development and indicates how effectively a compound kills cancer cells while sparing healthy ones, based on the ratio of toxic to effective concentrations. It is defined as the ratio of a compound's cytotoxicity toward normal cells (IC_{50} HdFn) to its cytotoxicity toward cancer cells. SI values above 1.0 indicate meaningful anticancer specificity, and substantially higher SI values reflect strong selectivity. However, compounds **19, 20** and **21** showed the highest selectivity indices in the series (SI = 2.2, 2.3 and 2.2 respectively), indicating lower toxicity toward HdFn normal cells compared with the other compounds (Fig. 3). Fig. 4 illustrated the anticancer activity of compounds **17–23** alongside tamoxifen as the reference drug, presented as IC_{50} values against MCF-7 cells and primary neonatal human dermal fibroblast (HDFn) cell lines.

3.2.2. Total antioxidant capacity (TAC)

TAC assays have been widely applied to biological samples to evaluate extracellular non-enzymatic antioxidants. Furthermore, total antioxidant activity (TAA) is important because it reflects the body's overall capacity to counteract oxidative stress, a major contributor to the development of many chronic diseases. Assessing TAA aids in diagnosis, prognosis, and in monitoring how well treatments are working across diverse health conditions. An example of such a case is oxidative DNA

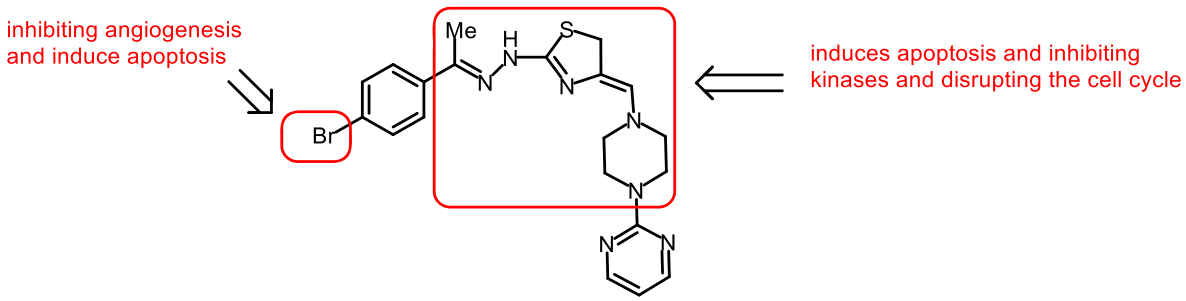

Fig. 3. Impact of *p*-bromophenyl, and hydrazinyl-4,5-dihydrothiazole moieties of compound **19** on its anticancer activity.

damage and its correlation with total antioxidant capacity (TAC) levels in patients with glioblastoma multiforme [56].

The total antioxidant capacity (TAC) of compounds **17–23** was measured by phosphomolybdate method [33] using ascorbic acid as a standard. The method relies on a reduction reaction where antioxidants transform molybdenum (VI) into molybdenum (V), resulting in a green complex that is quantified using spectrophotometry. The pattern of electron or hydrogen donation by antioxidants is influenced by their structural features and the series of redox reactions associated with their activity. As shown in Table 2, compound **21** showed the strongest antioxidant activity (particularly at the highest concentration tested (250 ug/mL), with a TAC value (27.270 ± 1.005 ug/mL) surpassing even ascorbic acid (A.A.) at the same concentration (TAC value = 18.521±0.336 ug/mL). In contrast, compounds **17**–**19** exhibited relatively lower antioxidant activity at the same concentrations compared with ascorbic acid. In addition, the very low activity observed for compounds **20, 22**, and **23** suggested that variations in their antioxidant mechanisms or structural characteristics may influence their performance. Overall antioxidant strength increased in the order **20** < **22** < **23** < **19** < **18** < **17** < **21** (weak → strong) (Table 2 and Fig. 5). The superior performance of compound **21** is attributed to its *para*-amino substituent, whose electron-donating effect enhances hydrogen-donation ability and free-radical.

3.2.3. Antifungal and antibacterial activity

The antibacterial activity of compounds **17–23** was evaluated against the Gram-negative bacterial strain *E.coli*(ATCC 25,922). The antibacterial activity of compounds **17**–**23** was assessed against the Gram-negative bacterial strain *E.coli*(ATCC 25,922). Antibacterial potency was determined based on the inhibition zone diameter (mm), using chloramphenicol (CHL) and clotrimazole (CLT) as reference drugs. Compound **21** exhibited exceptional activity against *E. coli*, showing an inhibition zone of 31.0 mm, which exceeded that of all other tested compounds and the reference drug chloramphenicol (CHL; inhibition zone = 26 mm). Furthermore, compounds **17–23** were also evaluated for their in vitro antifungal activity against *Candida albicans* (*C. albicans* SC5314), using well diffusion method to determine the inhibition zone in mm. Among the screened derivatives, compound **21** was the most active, exhibiting an inhibition zone of 26 mm against *C. albicans*, compared with 24 mm for the reference drug clotrimazole (CLT) Table 3.

4. In silico studies

4.1. Docking study

Redocking of the native ligands into their respective receptor binding sites produced RMSD values of 0.881 Å for ERα (1ERR) and 1.093 Å for EGFR (3W2S), both well below the accepted threshold of 2.0 Å (Fig. 6), supporting the reliability of the docking parameters and scoring functions used in this study.

Tamoxifen exhibited strong binding toward both targets with docking scores of −10.61 kcal.mol^{-1} for ERα and −7.92 kcal.mol^{-1} for EGFR (Table 4). Among the tested derivatives, compound **19** demonstrated the most favorable binding energies (−10.04 kcal.mol^{-1} for both receptors), approaching that of tamoxifen. Compounds **17** and **22** also displayed significant affinities (−9.92 to −9.84 kcal.mol^{-1}).

These results are consistent with the in vitro cytotoxicity data obtained against the MCF-7 breast cancer cell line, where derivative **19** demonstrated the highest antiproliferative effect and a selectivity index (SI) of 2.2. The improved binding of ligand **19** is likely due to its *p*-bromophenyl and hydrazinyl-4,5-dihydrothiazole substituents, which enhance its molecular complementarity within both receptor active sites. While these findings suggest that compound **19** may interact with both ERα and EGFR, experimental validation is required to confirm dual-target activity. The current evidence is based exclusively on in silico predictions; therefore, techniques such as Western blotting, RT-PCR, or immunofluorescence would be necessary to verify whether these interactions truly modulate ERα/EGFR signaling in biological systems.

As shown in Fig. 7, tamoxifen forms a hydrogen bond with Thr A:41 and engages in π–sulfur interactions with Met A:114 within the ERα binding pocket, complemented by hydrophobic contacts with Leu A:40, Leu A:43, Ala A:44, Leu A:77, Leu A:80, Leu A:84, Phe A:97, and Leu A:208. Likewise, Compound **19** establishes hydrogen bonds with Ala A:44 and Gly A:204, π–sulfur interactions with Arg A:87 and Phe A:97, and hydrophobic interactions involving Leu A:80, Met A:81, Leu A:84, Met A:114, Ile A:117, and Leu A:208.

Within the EGFR kinase domain (PDB ID: 3W2S), tamoxifen forms hydrogen bonds with Lys A:45, Thr A:154, Asp A:155, and Phe A:156, as well as hydrophobic interactions with Leu A:18, Phe A:23, Val A:26, Ala A:43, Leu A:47, Met A:66, Leu A:77, Leu A:88, and Leu A:158 (Fig. 7). Conversely, compound **19** interacts through a hydrogen bond with Cys A:75, π–anion interactions with Lys A:45 and Asp A:155, and hydrophobic contacts involving Val A:26, Ala A:43, Ahr A:90, and Leu A:144, indicating its stable accommodation within the ATP-binding cleft.

4.2. ADMET analysis

The ADMET evaluation provides crucial insights into the pharmacokinetic, drug-likeness, and toxicity profiles of the synthesized compounds **17**–**23** compared with the reference drug tamoxifen (TMX) (Table 5). All compounds displayed moderate to good aqueous solubility, with ranging from −4.51 to −5.49 mol/L, indicating acceptable formulation potential. In terms of absorption, the tested derivatives exhibited high Caco-2 permeability (0.79–1.04 log Papp) and GI absorption rates above 78 %, indicating efficient intestinal uptake comparable to TMX (96.9 %). All molecules were predicted to be P-glycoprotein substrates, suggesting possible efflux transport involvement but not severe restriction in bioavailability [57].

In terms of distribution, the predicted steady-state volume of distribution (VDss) values (−0.27 to 0.12 log L/kg) indicate moderate tissue distribution, whereas tamoxifen (TMX) shows a higher VDss (0.83 log L/kg), consistent with more extensive tissue penetration [58,59]. The predicted blood–brain barrier (BBB) permeability values (log BB =

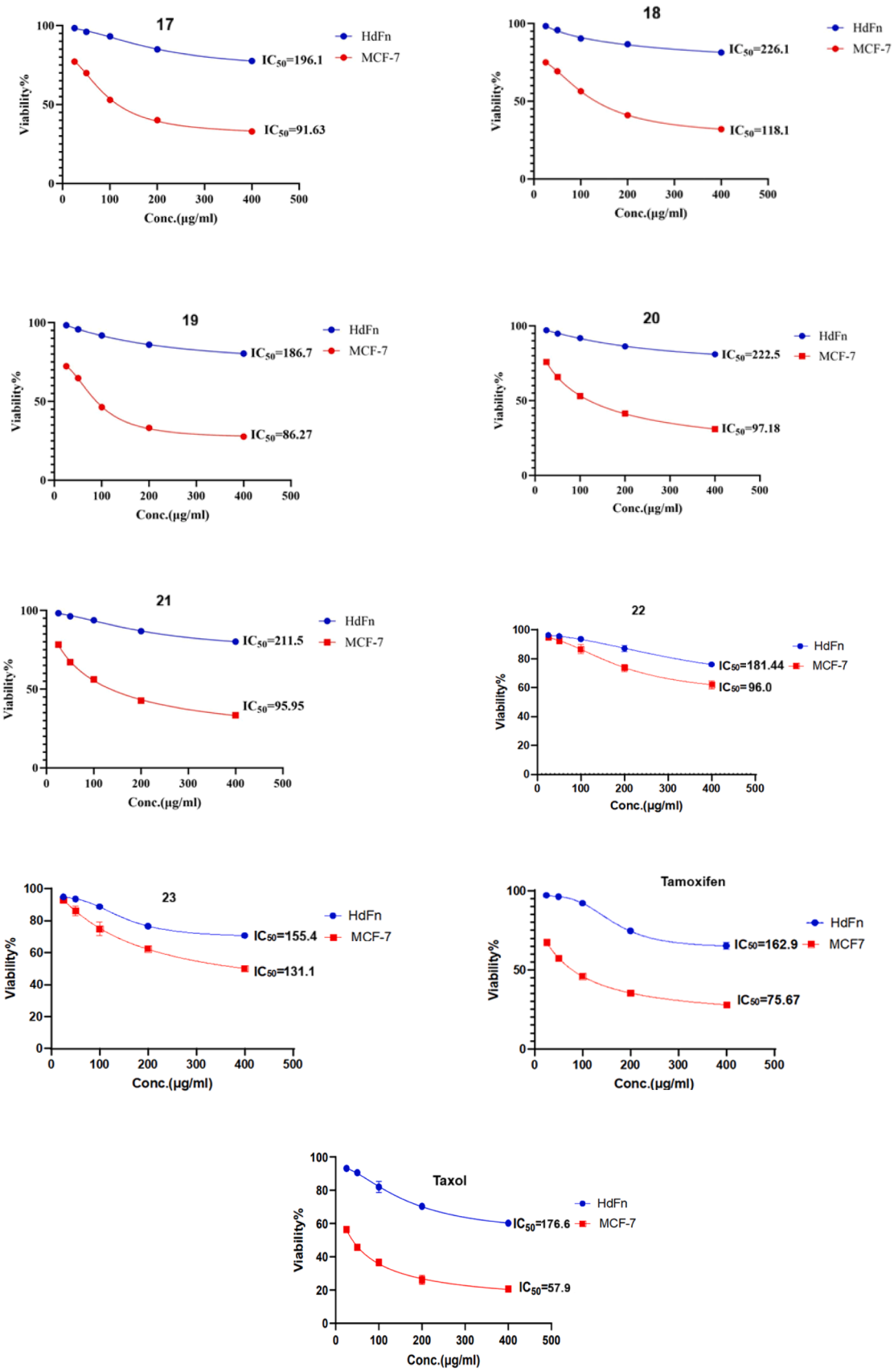

Fig. 4. Cell viability % of MCF-7 cell line against compounds **17–23**, tamoxifen and taxol on MCF-7 and HdFn normal cells, after 72 h incubation at $T = 37$ °C. The assays were performed in triplicate.

Table 2
Total antioxidant capacity (%) of 2-(piperazin-1-yl) derivatives **17–23.**

Compd.	Conc. (ug/mL) mean±SD (%)				
	250	200	150	100	50
17	22.877 ±0.214	16.892±0.401	14.961 ±0.259	13.521 ±0.259	7.007 ±0.507
18	21.816 ±0.446	18.597±0.259	15.339 ±0.398	12.044 ±0.361	5.037 ±0.191
19	20.036 ±0.312	16.514±0.277	14.733 ±0.259	6.136 ±0.401	2.916 ±0.469
20	16.635 ±0.923	13.938±0.327	6.401 ±0.398	1.894 ±0.262	0.341 ±0.287
21	27.270 ±1.005	23.789±0.391	18.521 ±0.379	15.036 ±0.469	12.423 ±0.942
22	17.536 ±0.501	14.052±0.544	11.287 ±0.612	4.469 ±0.502	1.098 ±0.259
23	18.521 ±0.336	14.468±0.727	8.333 ±0.410	1.856 ±0.191	0.606 ±0.214
A.A.	25.215 ±0.145	22.141±0.231	18.216 ±0.291	15.150 ±0.184	12.131 ±0.115

A.A.: Ascorbic acid.

−0.51 to −1.03) show that the new derivatives are unlikely to cross the central nervous system (CNS), which is advantageous in limiting potential neurological side effects. Consistently, the CNS permeability values (log PS ≈ −2.2 to −2.5) further support their restricted brain exposure.

Regarding metabolism, all derivatives were predicted to be CYP3A4 substrates, indicating that hepatic Phase I biotransformation is primarily mediated through this isoenzyme. Importantly, none of the compounds inhibited the major CYP isoforms (CYP1A2, 2C9, 2C19, 2D6, 3A4), except compound **20**, which showed mild CYP3A4 inhibition. This contrasts with TMX, which inhibits CYP1A2 and CYP2D6 and therefore carries a higher potential for drug–drug interactions [60]. For compound **19** in particular, its CYP3A4-substrate status combined with the absence of CYP inhibition suggests predictable metabolism with a reduced likelihood of metabolic interference.

During the excretion phase, the predicted total clearance values (0.12–0.35 log mL/min/kg) reflect moderate elimination rates, comparable to tamoxifen (0.556). Additionally, none of the compounds were predicted to be renal OCT2 substrates, indicating that renal tubular secretion likely does not play a major role in their elimination [61].

The toxicity assessment revealed that all derivatives fall into toxicity class 4, indicating low acute toxicity with LD_{50} values ranging from 2.39 to 2.98 mol/kg. All compounds were predicted to be non-mutagenic (negative AMES test), except for compound **20** and tamoxifen (TMX), which exhibited mutagenic potential. None of the new derivatives were predicted to inhibit hERG I channels, suggesting a low risk of cardiotoxicity, whereas TMX tested positive for hERG I inhibition. Furthermore, all derivatives were predicted to be non-hepatotoxic, in contrast to TMX, which showed a 69 % probability of hepatotoxicity.

Regarding carcinogenicity, compounds **18** and **20–23** displayed a

Table 3
Diameter of zones of inhibition (mm) of compounds **17–23** against *E. coli* and *C. albicans.*

Compd.	*E. coli* (Inhib. zone, mm)	*C. albicans* (Inhib. zone, mm)
17	26	18
18	22	7
19	20	20
20	15	23
21	31	26
22	22	22
23	23	23
CHL	26	-
CLT	-	24

CHL: Chloramphenicol; CLT: Clotrimazole.

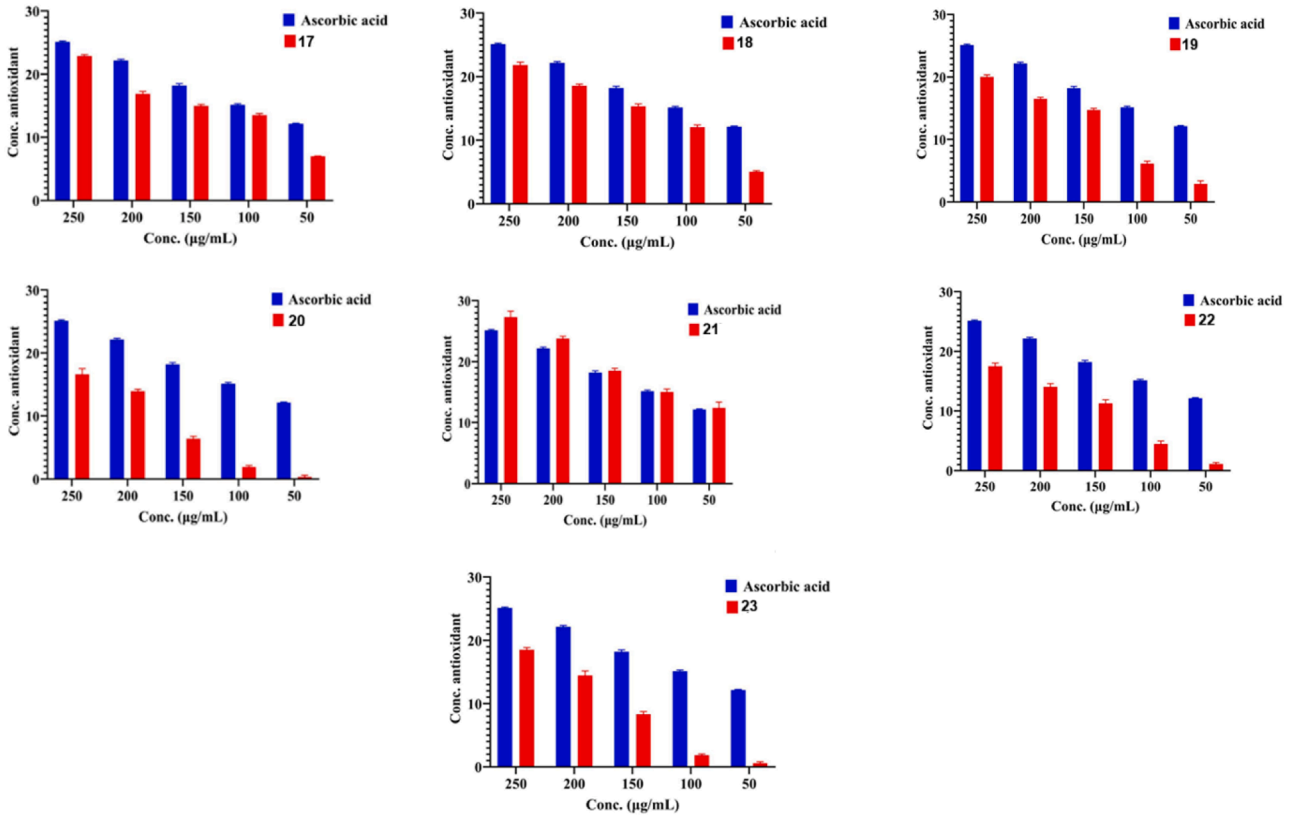

Fig. 5. Histogram representing the antioxidant activity of compounds **17–23**.

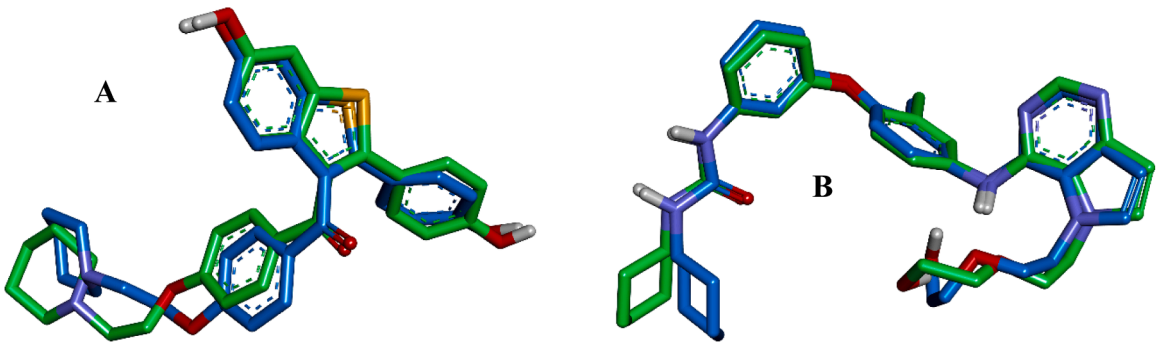

Fig. 6. Superimposition of native ligands (green) and their redocked poses (blue) within the active sites of (A) ERα (1ERR) and (B) EGFR (3W2S).

Table 4
RMSD (Å) and binding energy (kcal/mol) values of compounds **17–23** and tamoxifen.

Ligand	1ERR	3W2S
RMSD	0.881	1.093
Native ligand	13.80	−13.76
TMX	−10.61	−7.92
19	−10.04	−10.04
17	−9.92	−9.79
22	−9.69	−9.84
23	−9.5	−9.25
21	−9.37	−9.38
18	−9.31	−9.21
20	−8.89	−9.06

moderate risk (56–77 %), while derivatives **17** and **19** showed no carcinogenic potential. Immunotoxicity predictions were positive for all derivatives a common observation among bioactive molecules with immunomodulatory activity. None of the compounds were predicted to cause skin sensitization or cytotoxicity. Overall, compound **19** demonstrated the most favorable ADMET profile, characterized by high absorption, good solubility, moderate clearance, low predicted toxicity, and lack of CYP inhibition. Combined with its strong binding affinity and potent in vitro anticancer activity, these attributes identify compound **19** as the most promising lead among the tested derivatives.

4.3. Molecular dynamics simulation

Molecular Dynamics simulations (MDS) were conducted for the most active compound **19** and the reference drug tamoxifen (TMX) in complex with both ERα (PDB ID: 1ERR) and EGFR (PDB ID: 3W2S) to assess the structural stability, flexibility, and compactness of ligand–protein systems over 100 ns. The simulation parameters, including RMSD, RMSF, Rg, and SASA, are summarized in Table 6 and illustrated in Fig. 8.

The RMSD analysis (Fig. 8) revealed that all complexes reached equilibrium rapidly and remained stable throughout the simulation. The ERα–**19** and ERα–TMX complexes displayed RMSD values of 0.183 nm and 0.164 nm, respectively, confirming that compound **19** maintained a stable conformation comparable to TMX within the ERα binding site. Likewise, the EGFR–**19** and EGFR–TMX complexes exhibited similar RMSD values (0.188 nm and 0.181 nm), indicating that both ligands stabilized the kinase domain without major structural deviation.

RMSF analysis showed low fluctuations (< 0.6 nm) across most residues for all systems, suggesting limited flexibility and stable interactions between ligand and key binding site residues. A slight increase in local fluctuations was observed for ERα upon **19** binding (0.151 nm vs 0.129 nm), likely reflecting adaptive side-chain rearrangements to accommodate the ligand. In contrast, EGFR exhibited a minor decrease in RMSF (0.139 nm for **19** vs 0.144 nm for TMX), implying reduced mobility and a stabilizing effect of compound **19**.

The SASA values (116–158 nm^2) exhibited only minor differences between TMX- and **19**-bound systems, indicating that ligand binding did not significantly affect solvent exposure or protein folding. A slight increase in SASA for both ERα–**19** and EGFR-**19** suggests minimal surface expansion due to local conformational adjustments during ligand accommodation. Similarly, Rg analysis confirmed that all protein–ligand complexes remained compact and structurally stable throughout the 100 ns simulation. The Rg values (1.787–2.048 nm) closely matched those of the native proteins, demonstrating that binding of derivative **19** does not disrupt protein compactness or tertiary structure integrity. Overall, the MDS results indicate that compound **19** forms dynamically stable complexes with both ERα and EGFR, maintaining comparable or slightly improved conformational stability relative to TMX. These findings underscore the strong binding affinity of compound **19** and reinforce its potential as a dual inhibitor of both receptors.

5. Conclusion

In this study, a series of 2-(2-(1-(4-aryl)ethylidene)hydrazinyl)-4-((4-(pyrimidin-2-yl)piperazin-1-yl)methylene)-4,5-dihydrothiazole derivatives **17–23** were successfully synthesized and evaluated for their biological potential. Among them, compound **19** emerged as the most promising antiproliferative candidate against MCF-7 breast cancer cells (IC_{50}= 86.27 ug/mL, SI = 2.2), while compound 21 exhibited the strongest antioxidant (TAC = 27.27 ± 1.01 ug/mL at 250 ug/mL), antibacterial (*E. coli*inhibition zone = 31 mm) and antifungal (*C. albicans* inhibition zone = 26 mm) activities, suggesting multifunctional bioactivity within this series. Molecular docking analyses showed that compound **19** binds strongly to both ERα and EGFR, with binding energies (−10.04 kcal/mol for both receptors) comparable to tamoxifen (−10.61 and −7.92 kcal/mol), and MD simulations confirmed stable ERα–**19** and EGFR–**19** complexes with low RMSD, compact Rg values and comparable SASA to the reference complexes over 100 ns. These computational findings , together with the superior in vitro antiproliferative effect, support compound **19** as a putative dual binder of ERα and EGFR, although this dual-target interaction remains a hypothesis that requires experimental validation. ADMET profiling indicated favorable pharmacokinetic and safety features, including high absorption, good solubility, and low predicted toxicity. Collectively, these findings highlight the therapeutic potential of the synthesized derivatives, with compound **19** as a promising lead scaffold for anticancer drug development, and compound **21** as a promising candidate for antioxidant and antimicrobial applications. Future work will focus on evaluating additional breast cancer cell lines, such as MDA-MB-231 and T-47D, alongside in vivo studies and mechanistic validation. This will include ERα/EGFR-related assays, as well as structural optimization to improve potency and selectivity.

CRediT authorship contribution statement

Nabeel A. Abdul-Rida: Methodology, Investigation,

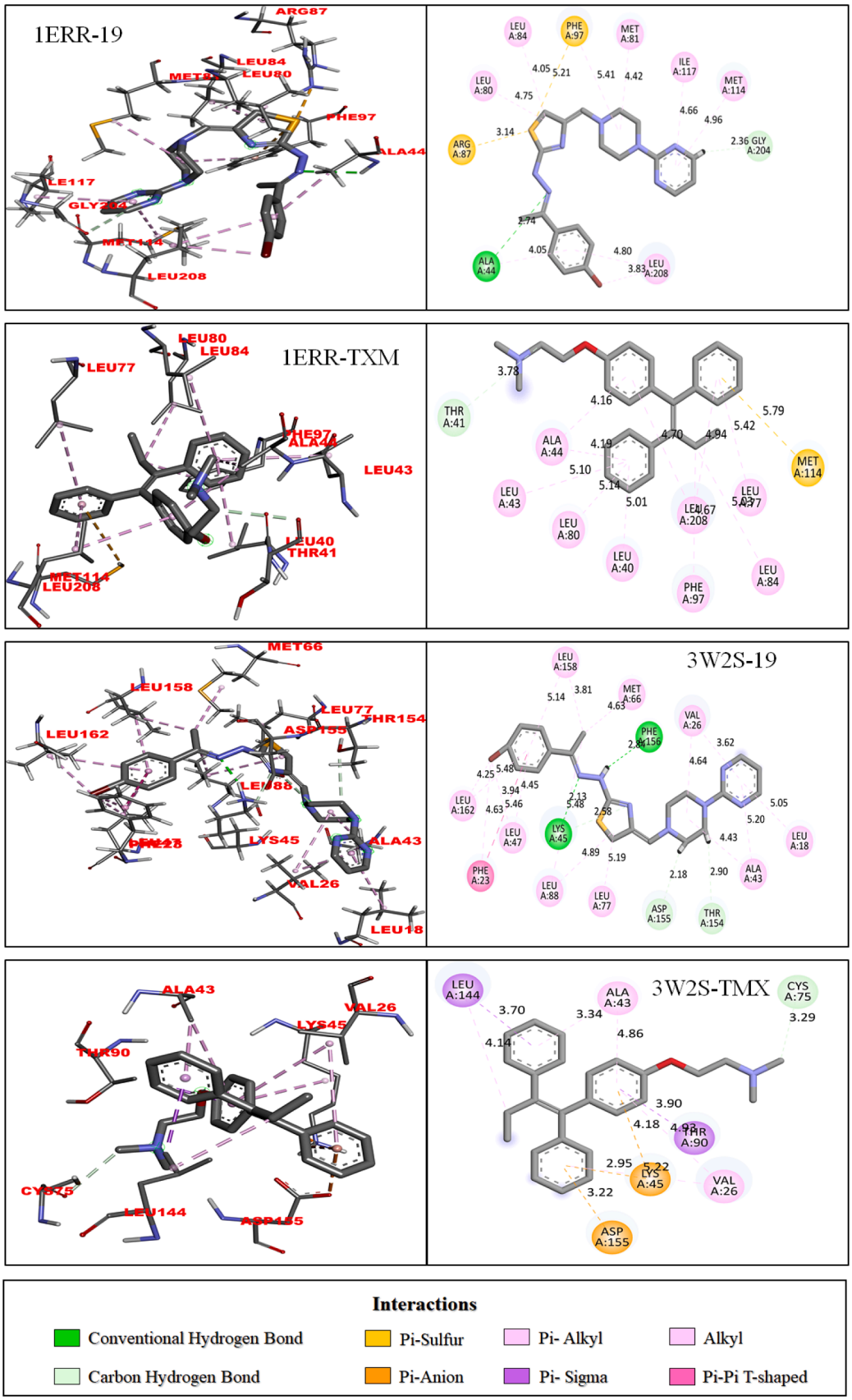

Fig. 7. 2D and 3D Binding interactions of compound **19** and TXM with the active sites of ERα and EGFR.

Table 5
ADMET parameters for compounds **17–23** and tamoxifen.

	C17	C18	C19	C20	C21	C22	C23	TMX
Water solubility (log mol/L)	−5.404	−4.516	−5.493	−4.798	−4.511	−4.916	−4.788	−5.929
Caco-2 permeability (log Papp in 10^{-6} cm/s)	0.963	1.044	0.959	0.792	0.890	0.997	0.981	1.065
GI absorption (%)	91.80	92.12	91.733	82.958	78.946	93.457	93.46	96.885
P-gp substrate	Yes	Yes	Yes	Yes	Yes	Yes	Yes	Yes
VDss (log L/kg)	−0.119	0.045	−0.106	−0.160	0.126	−0.267	−0.089	0.830
BBB permeability (log BB)	−0.66	−1.038	−0.668	−0.938	−0.913	−0.703	−0.508	1.329
CNS permeability (log PS)	−2.238	−2.542	−2.215	−2.580	−2.527	−2.517	−2.352	−1.473
CYP3A4 substrate	Yes	Yes	Yes	Yes	Yes	Yes	Yes	Yes
CYP1A2 inhibitor	No	No	No	No	No	No	No	Yes
CYP2C19 inhibitor	No	No	No	No	No	No	No	No
CYP2C9 inhibitor	No	No	No	No	No	No	No	No
CYP2D6 inhibitor	No	No	No	No	No	No	No	Yes
CYP3A4 inhibitor	No	No	No	Yes	No	No	No	No
Total Clearance (log mL/min/kg)	0.221	0.120	0.199	0.257	0.120	0.269	0.352	0.556
Renal OCT2 substrate	No	No	No	No	No	No	No	No
LD_{50} (mol/kg)	2.981	2.392	2.975	2.656	2.667	2.864	2.940	2.285
Toxicity class	4	4	4	4	4	4	4	4
AMES	No	No	No	Yes	No	No	No	Yes
hERG I inhibitor	No	No	No	No	No	No	No	Yes
Skin sensitisation	No	No	No	No	No	No	No	No
Hepatotoxicity	No 57 %	No 63 %	No 58 %	No 60 %	No 63 %	No 63 %	No 65 %	Yes 69 %
Carcinogenicity	No 53 %	Yes 59 %	No 51 %	Yes 77 %	Yes 62 %	Yes 56 %	Yes 58 %	No 62 %
Immunotoxicity	Yes 87 %	Yes 78 %	Yes 91 %	Yes 89 %	Yes 71 %	Yes 95 %	Yes 61 %	Yes 96 %
Mutagenicity	No 56 %	No 55 %	No 55 %	Yes 80 %	No 51 %	No 52 %	No 54 %	No 97 %
Cytotoxicity	No 52 %	No 53 %	No 54 %	No 59 %	No 50 %	No 55 %	No 54 %	No 93 %

Table 6
MDS results for compound **19** and TMX (NL) of ERα and EGFR.

	1ERR-TMX	1ERR-19	3W2S-TMX	3W2S-19
RMSD (nm)	0.164	0.183	0.181	0.188
RMSF (nm)	0.129	0.151	0.144	0.139
SASA (nm^2)	116.795	117.310	157.484	158.180
Rg (nm)	1.799	1.787	2.035	2.048

Conceptualization. **Noor H. Youssef:** Software, Methodology, Data curation. **Risala H. Allami:** Methodology, Investigation, Formal analysis, Data curation. **Yahia Bekker:** Visualization, Validation, Formal analysis, Data curation, Conceptualization. **Lanez Elhafnaoui:** Writing – original draft, Visualization, Validation, Investigation, Data curation, Conceptualization. **Najim A. Al-Masoudi:** Writing – review & editing, Writing – original draft, Supervision, Project administration, Methodology, Investigation, Formal analysis, Data curation, Conceptualization.

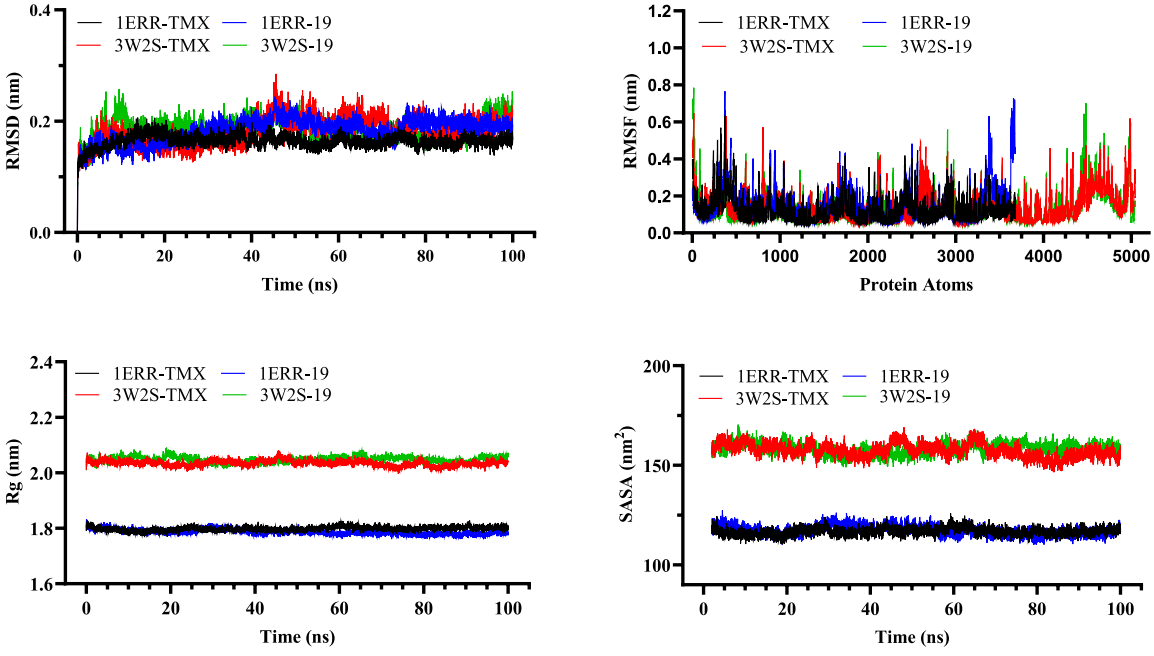

Fig. 8. MDS trajectories of ERα and EGFR complexes with compound **19** and TMX over 100 ns.

Declaration of competing interest

The authors declare that they have no known competing financial interests or personal relationships that could have appeared to influence the work reported in this paper.

Supplementary materials

Supplementary material associated with this article can be found, in the online version, at doi:10.1016/j.molstruc.2026.145287.

Data availability

No data was used for the research described in the article.

References

[1] V. Battisti, J. Moesslacher, R. Abdelnabi, P. Leyssen, A.L. Rosales Rosas, L. Langendries, M. Aufy, C. Studenik, J.M. Kratz, J.M. Rollinger, G. Puerstinger, J. Neyts, L. Delang, E. Urban, T. Langer, Design, synthesis, and lead optimization of piperazinyl-pyrimidine analogues as potent small molecules targeting the viral capping machinery of chikungunya virus, Eur. J. Med. Chem. 264 (2024) 116010, https://doi.org/10.1016/j.ejmech.2023.116010.

[2] B. Nammalwar, R.A. Bunce, Recent advances in pyrimidine-based drugs, Pharmaceuticals 17 (2024) 104, https://doi.org/10.3390/ph17010104.

[3] B. Vavaiya, S. Patel, V. Pansuriya, V. Marvaniya, P. Patel, Synthesis, anti-tubercular evaluation and molecular docking studies of nitrogen-rich piperazine-pyrimidine-pyrazole Hybrid motifs, Curr. Chem. Lett. 11 (2022) 95–104, https://doi.org/10.5267/j.ccl.2021.9.001.

[4] W.A. Al-Masoudi, N.A. Al-Masoudi, A ruthenium complexes of monastrol and its pyrimidine analogues: synthesis and biological properties, Phosphorus. Sulfur. Silicon. Relat. Elem. 194 (2019), https://doi.org/10.1080/10426507.2019.1597362, 102-27.

[5] F.A.K. Almashal, H.H. Al-Hujaj, A.M. Jassem, N.A. Al-Masoudi, A click synthesis, molecular docking, cytotoxicity on breast cancer (MDA-MB 231) and anti-HIV activities of new 1,4-dsubstituted-1,2,3-triazole thymine derivatives, Russ. J. Bioorg. Chem. 46 (2020) 360–370, https://doi.org/10.1134/S1068162020030024.

[6] W.A. Al-Masoudi, N.A. Al-Masoudi, B. Weibert, R. Winter, Synthesis, X-ray structure, in vitro HIV and kinesin Eg5 inhibition activities of new arene ruthenium complexes of pyrimidine analogs, J. Coord. Chem. 70 (2017), https://doi.org/10.1080/00958972.2017.1334259, 2061-73.

[7] N.A. Abdul-Rida, T.I. Mohammed, N.A. Al-Masoudi, M. Frotscher, Synthesis, anti-17β-HSD and antiproliferative activity of new substituted 5-nitrosopyrimidine analogs, Med. Chem. Res. 26 (2017) 830–840, https://doi.org/10.1007/s00044-017-1795-z.

[8] H.A. Al-Hazam, Z.A. Al-Shamkani, N.A. Al-Masoudi, B.A. Saeed, C. Pannecouque, New chalcones and thiopyrimidine analogues derived from mefenamic acid: microwave-assisted synthesis, anti-HIV activity and cytotoxicity as antileukemic agents, Z. Naturforsch. B 72 (2017) 249–256, https://doi.org/10.1515/znb-2016-0223.

[9] S. Iacob Ciobotaru, C.-S. Stefan, A. Nechita, M.-N. Matei, E.-L. Lisa, D. Tutunaru, I. Fulga, A. Fulga, A.-G. Cristea Hohota, O.-M. Dragostin, Hybrid molecules with purine and pyrimidine derivatives for antitumor therapy: news, perspectives, and future directions, Molecules 30 (2025) 2707, https://doi.org/10.3390/molecules30132707.

[10] S. Rejinthala, S. Endoori, D. Vemula, V. Bhandari, T. Mondal, Novel pyrimidine-piperazine hybrids as potential antimicrobial agents: in-vitro antimicrobial and in-silico studies, Results. Chem. 5 (2023) 100951, https://doi.org/10.1016/j.rechem.2023.100951.

[11] R. Shivakumar, G. Sethi, K. Manikanta, Z. Xi, A. Ravish, P.M. Uppar, S. N. Deveshegowda, A.M. Kumar, S. Basappa, C.S. Bhol, S.L. Gaonkar, K. Kemparaju, A. Chinnathambi, S.A. Alharbi, P.E. Lobie, V. Pandey, B. Basappa, Discovery of piperazin-2-yl-pyrimidines as anticancer agents via targeting JNK signaling pathway in human MCF-7 breast carcinoma, ChemistrySelect 9 (2024) e202400307, https://doi.org/10.1002/slct.202400307.

[12] A. Kładna, P. Berczyński, O.B. Dündar, M.C. Ünlüsoy, E. Sarı, B. Bakinowska, I. Kruk, H.Y. Aboul-Enein, Synthesis and in vitro antioxidant activity of new pyrimidin/benzothiazol-substituted piperazinyl flavones, Future Med. Chem. 10 (2018) 2293, https://doi.org/10.4155/fmc-2018-0206. -08.

[13] B. Kaya, L. Yurttaş, B.N. Sağlik, S. Levent, Y. Özkay, Z.A. Kaplancikli, Novel 1-(2-pyrimidin-2-yl)piperazine derivatives as selective monoamine oxidase (MAO)-A inhibitors, J. Enzyme Inhib. Med. Chem. 32 (2017) 193–202, https://doi.org/10.1080/14756366.2016.1247054.

[14] F. Kayamba, R. Karpoormath, V.A. Obakachi, M. Mahlalela, D. Banda, R.L. van Zyl, S. Lala, T. Zininga, A. Shonhai, B.B. Shaik, O.J. Pooe, A promising class of antiprotozoal agents, design and synthesis of novel pyrimidine–cinnamoyl hybrids, Eur. J. Med. Chem. 281 (2025) 116944, https://doi.org/10.1016/j.ejmech.2024.116944.

[15] A. Newman-Tancredi, J.-P. Nicolas, V. Audinot, S. Gavaudan, L. Verrièle, M. Touzard, C. Chaput, N. Richard, M.J. Millan, Actions of α2 adrenoceptor ligands at α2A and 5-HT1A receptors: the antagonist, atipamezole, and the agonist, dexmedetomidine, are highly selective for α2A adrenoceptors, Naunyn. Schmiedebergs. Arch. Pharmacol. 358 (1998) 197–206, https://doi.org/10.1007/PL00005243.

[16] A. Bronowska, A. Leś, M. Mazgajska, Z. Chilmończyk, Conformational analysis and pharmacophore design for selected 1-(2-pyrimidinyl)piperazine derivatives with sedative-hypnotic activity, Acta Pol. Pharm. 58 (2001) 79–86. http://www.ncbi.nlm.nih.gov/pubmed/11501794.

[17] M. Al-Ghorbani, M.A. Gouda, M. Baashen, L. Ranganatha, Pyrimidine-piperazine hybrids; recent synthesis and biological activities, Polycycl. Aromat. Compd. 42 (2022) 7187, https://doi.org/10.1080/10406638.2021.1998144. -16.

[18] F.R. Luo, Z. Yang, A. Camuso, R. Smykla, K. McGlinchey, K. Fager, C. Flefleh, S. Castaneda, I. Inigo, D. Kan, M.-L. Wen, R. Kramer, A. Blackwood-Chirchir, F. Y. Lee, Dasatinib (BMS-354825) pharmacokinetics and pharmacodynamic biomarkers in animal models predict optimal clinical exposure, Clin. Cancer Res. 12 (2006) 7180–7186, https://doi.org/10.1158/1078-0432.CCR-06-1112.

[19] L.J. Lombardo, F.Y. Lee, P. Chen, D. Norris, J.C. Barrish, K. Behnia, S. Castaneda, L. A.M. Cornelius, J. Das, A.M. Doweyko, C. Fairchild, J.T. Hunt, I. Inigo, K. Johnston, A. Kamath, D. Kan, H. Klei, P. Marathe, S. Pang, R. Peterson, S. Pitt, G.L. Schieven, R.J. Schmidt, J. Tokarski, M.-L. Wen, J. Wityak, R.M. Borzilleri, Discovery of N-(2-chloro-6-methyl-phenyl)-2-(6-(4-(2-hydroxyethyl)-piperazin-1-yl)-2-methylpyrimidin-4-ylamino)thiazole-5-carboxamide (BMS-354825), a dual Src/Abl kinase inhibitor with potent antitumor activity in preclinical assays, J. Med. Chem. 47 (2004) 6658–6661, https://doi.org/10.1021/jm049486a.

[20] G.M. Keating, Dasatinib: a review in chronic myeloid leukaemia and ph+ acute lymphoblastic leukaemia, Drugs 77 (2017) 85–96, https://doi.org/10.1007/s40265-016-0677-x.

[21] U. Rix, O. Hantschel, G. Dürnberger, L.L. Remsing Rix, M. Planyavsky, N. V. Fernbach, I. Kaupe, K.L. Bennett, P. Valent, J. Colinge, T. Köcher, G. Superti-Furga, Chemical proteomic profiles of the BCR-ABL inhibitors imatinib, nilotinib, and dasatinib reveal novel kinase and nonkinase targets, Blood 110 (2007) 4055–4063, https://doi.org/10.1182/blood-2007-07-102061.

[22] S. Redaelli, R. Piazza, R. Rostagno, V. Magistroni, P. Perini, M. Marega, C. Gambacorti-Passerini, F. Boschelli, Activity of bosutinib, dasatinib, and nilotinib against 18 imatinib-resistant BCR/ABL mutants, J. Clin. Oncol. 27 (2009) 469–471, https://doi.org/10.1200/JCO.2008.19.8853.

[23] J.D. Rowley, A new consistent chromosomal abnormality in chronic myelogenous leukaemia identified by quinacrine fluorescence and giemsa staining, Nature 243 (1973) 290–293, https://doi.org/10.1038/243290a0.

[24] J.S. Tokarski, J.A. Newitt, C.Y.J. Chang, J.D. Cheng, M. Wittekind, S.E. Kiefer, K. Kish, F.Y.F. Lee, R. Borzillerri, L.J. Lombardo, D. Xie, Y. Zhang, H.E. Klei, The structure of dasatinib (BMS-354825) bound to activated ABL kinase domain elucidates its inhibitory activity against imatinib-resistant ABL mutants, Cancer Res. 66 (2006) 5790–5797, https://doi.org/10.1158/0008-5472.CAN-05-4187.

[25] S. Nam, D. Kim, J.Q. Cheng, S. Zhang, J.-H. Lee, R. Buettner, J. Mirosevich, F. Y. Lee, R. Jove, Action of the Src family kinase inhibitor, dasatinib (BMS-354825), on human prostate cancer cells, Cancer Res. 65 (2005) 9185–9189, https://doi.org/10.1158/0008-5472.CAN-05-1731.

[26] T. Chen, C. Wang, Q. Liu, Q. Meng, H. Sun, X. Huo, P. Sun, J. Peng, Z. Liu, X. Yang, K. Liu, Dasatinib reverses the multidrug resistance of breast cancer MCF-7 cells to doxorubicin by downregulating P-gp expression via inhibiting the activation of ERK signaling pathway, Cancer Biol. Ther. 16 (2015) 106–114, https://doi.org/10.4161/15384047.2014.987062.

[27] N.A. Abdul-Ridha, A.M. Youssef, L. Elhafnaoui, Y. Bekker, N.A. Al-Masoudi, B. A. Saeed, W.A. Al-Masoudi, Synthesis, in-silico evaluation, ADME analysis, and molecular dynamics simulation of novel β-lactam derivatives based on diclofenac and sulindac with anticancer and antioxidant activities, Chem. Biodivers. (2025) e01586, https://doi.org/10.1002/cbdv.202501586.

[28] S. Asghar, S. Hameed, N.A. Al-Masoudi, B. Saeed, A. Shtaiwi, Design, synthesis, docking studies and molecular dynamics simulation of new 1,3,5-triazine derivatives as anticancer agents selectively targeting pancreatic adenocarcinoma (Capan-1), Chem. Biodivers. 21 (2024) e202400112, https://doi.org/10.1002/cbdv.202400112.

[29] N.A. Al-Masoudi, Y.A. Al-Soud, A. Kalogerakis, C. Pannecouque, E. De Clercq, Nitroimidazoles part 2. Synthesis, antiviral and antitumor activity of new 4-nitroimidazoles, Chem. Biodivers. 3 (2006) 515–526, https://doi.org/10.1002/cbdv.200690055.

[30] S. Asghar, A. Aziz, S. Hameed, B.A. Saeed, R.H. Allami, N.A. Al-Masoudi, Synthesis of novel 1,3,5-triazine analogues with selective activity against pancreatic (Capan-1) and colorectal (HCT-116) carcinomas: anticancer potential and DNA-binding affinity, Chem. Biodivers. (2025) e01362, https://doi.org/10.1002/cbdv.202501362.

[31] S. Gupta, D. Pandey, D. Mandalapu, V. Bala, V. Sharma, M. Shukla, S.K. Yadav, N. Singh, S. Jaiswal, J.P. Maikhuri, J. Lal, M.I. Siddiqi, G. Gupta, V.L. Sharma, Design, synthesis and biological profiling of aryl piperazine based scaffolds for the management of androgen sensitive prostatic disorders, Medchemcomm 7 (2016) 2111–2121, https://doi.org/10.1039/C6MD00426A.

[32] T. Mosmann, Rapid colorimetric assay for cellular growth and survival: application to proliferation and cytotoxicity assays, J. Immunol. Methods 65 (1983) 55–63, https://doi.org/10.1016/0022-1759(83)90303-4.

[33] P. Prieto, M. Pineda, M. Aguilar, Spectrophotometric quantitation of antioxidant capacity through the formation of a phosphomolybdenum complex: specific application to the determination of vitamin E, Anal. Biochem. 269 (1999) 337–341, https://doi.org/10.1006/abio.1999.4019.

[34] S. Magaldi, S. Mata-Essayag, C. Hartung de Capriles, C. Perez, M.T. Colella, C. Olaizola, Y. Ontiveros, Well diffusion for antifungal susceptibility testing, Int. J. Infect. Dis. 8 (2004) 39–45, https://doi.org/10.1016/j.ijid.2003.03.002.
[35] G.M. Morris, R. Huey, W. Lindstrom, M.F. Sanner, R.K. Belew, D.S. Goodsell, A. J. Olson, AutoDock4 and AutoDockTools4: automated docking with selective receptor flexibility, J. Comput. Chem. 30 (2009) 2785–2791, https://doi.org/10.1002/jcc.21256.
[36] M.D. Hanwell, D.E. Curtis, D.C. Lonie, T. Vandermeersch, E. Zurek, G.R. Hutchison, Avogadro: an advanced semantic chemical editor, visualization, and analysis platform, J. Cheminform. 4 (2012) 17, https://doi.org/10.1186/1758-2946-4-17.
[37] S. Kim, J. Chen, T. Cheng, A. Gindulyte, J. He, S. He, Q. Li, B.A. Shoemaker, P. A. Thiessen, B. Yu, L. Zaslavsky, J. Zhang, E.E. Bolton, PubChem 2023 update, Nucleic. Acids. Res. 51 (2023) D1373–D1380, https://doi.org/10.1093/nar/gkac956.
[38] H.M. Berman, The protein data bank, Nucleic. Acids. Res. 28 (2000) 235–242, https://doi.org/10.1093/nar/28.1.235.
[39] Y. Bekkar, E. Lanez, T. Lanez, L. Bourougaa, A. Adaika, Z. Saada, A. Benine, Antidiabetic potential of synthesized ferrocenylmethylaniline derivatives: insights from in vitro studies, molecular docking, ADMET, DFT calculations, and molecular dynamics simulation, Biotechnol. Appl. Biochem. (2025), https://doi.org/10.1002/bab.70014 (Online ahead of print)z.
[40] O. Boudebia, M.L. Benamor, L. Bourougaa, Y. Bekkar, E. Lanez, A. Adaika, R. Bouraoui, K. Nesba, H. Chaoua, S.E. Hachani, L. Bechki, T. Lanez, Holistic investigation of cotula cinerea essential oil against diabetes: hypoglycemic activity, enzymatic inhibition, GC–MS characterization, ADMET forecasting, MD simulations, and DFT insights, J. Comput. Aided. Mol. Des. 39 (2025) 80, https://doi.org/10.1007/s10822-025-00664-7.
[41] A. Adaika, Y. Bekkar, S. Youmbai, L. Bourougaa, E. Lanez, M.L. Ben Amor, K. Nesba, T. Lanez, L. Bechki, Synthesis, antioxidant, and antidiabetic potential of ferrocenylmethylnucleobase compounds: in vitro, in silico molecular docking, DFT calculation, and molecular dynamic simulations, Appl. Organomet. Chem. 39 (2025), https://doi.org/10.1002/aoc.7988.
[42] M.L. Ben Amor, E. Lanez, Y. Bekkar, A. Adaika, T. Lanez, K. Nesba, L. Bechki, Exploring the interactions of ferrocenylmethylnucleobase derivatives with BSA and HHb: insights from electrochemical, spectroscopic, ADMET, in silico docking, and MD simulations, ChemistrySelect. 10 (2025) 1–16, https://doi.org/10.1002/slct.202404678.
[43] Y. Bekkar, E. Lanez, T. Lanez, L. Bourougaa, A. Adaika, A. Benine, Z. Saada, Combined in vitro and in silico analysis of ferrocenylmethylaniline derivatives: antibacterial potential, DFT calculations, and molecular dynamics insights, J. Organomet. Chem. 1032 (2025) 123618, https://doi.org/10.1016/j.jorganchem.2025.123618.
[44] BIOVIA, Dassault Systèmes, Discovery Studio Visualizer, v21.1.0.20298; San Diego: Dassault Systèmes, (2020). https://discover.3ds.com/discovery-studio-visualizer-download (accessed February 18, 2025).
[45] A. Daina, O. Michielin, V. Zoete, SwissADME: a free web tool to evaluate pharmacokinetics, drug-likeness and medicinal chemistry friendliness of small molecules, Sci. Rep. 7 (2017) 42717, https://doi.org/10.1038/srep42717.
[46] D.E.V. Pires, T.L. Blundell, D.B. Ascher, pkCSM: predicting small-molecule pharmacokinetic and toxicity properties using graph-based signatures, J. Med. Chem. 58 (2015) 4066–4072, https://doi.org/10.1021/acs.jmedchem.5b00104.
[47] P. Banerjee, A.O. Eckert, A.K. Schrey, R. Preissner, ProTox-II: a webserver for the prediction of toxicity of chemicals, Nucleic. Acids. Res. 46 (2018) W257–W263, https://doi.org/10.1093/nar/gky318.
[48] D. Van Der Spoel, E. Lindahl, B. Hess, G. Groenhof, A.E. Mark, H.J.C. Berendsen, GROMACS: fast, flexible, and free, J. Comput. Chem. 26 (2005) 1701–1718, https://doi.org/10.1002/jcc.20291.
[49] V. Zoete, M.A. Cuendet, A. Grosdidier, O. Michielin, SwissParam: a fast force field generation tool for small organic molecules, J. Comput. Chem. 32 (2011) 2359–2368, https://doi.org/10.1002/jcc.21816.
[50] J. Huang, A.D. MacKerell, CHARMM36 all-atom additive protein force field: validation based on comparison to NMR data, J. Comput. Chem. 34 (2013) 2135–2145, https://doi.org/10.1002/jcc.23354.
[51] M. Xiabing, K. Ablajan, M. Obul, M. Seydimemet, R. Ruzi, L. Wenbo, Facial one-pot, three-component synthesis of thiazole compounds by the reactions of aldehyde/ketone, thiosemicarbazide and chlorinated carboxylic ester derivatives, Tetrahedron 72 (2016) 2349–2353, https://doi.org/10.1016/j.tet.2016.03.053.
[52] W. Willker, D. Leibfritz, R. Kerssebaum, W. Bermel, Gradient selection in inverse heteronuclear correlation spectroscopy, Mag. Reson. Chem. 31 (1993) 287–292, https://doi.org/10.1002/mrc.1260310315.
[53] A.T. Jannuzzi, A.M. Yilmaz Goler, N. Bayrak, M. Yıldız, H. Yıldırım, B. Karademir Yilmaz, D. Shilkar, R.J. Venkatesan, V. Jayaprakash, A.F. TuYuN, Exploring the anticancer effects of brominated plastoquinone analogs with promising cytotoxic activity in MCF-7 breast cancer cells via cell cycle arrest and oxidative stress induction, Pharmaceuticals 15 (2022) 777, https://doi.org/10.3390/ph15070777.
[54] E. Guenin, D. Ledoux, O. Oudar, M. Lecouvey, M. Kraemer, Structure-activity relationships of a new class of aromatic bisphosphonates that inhibit tumor cell proliferation in vitro, Anticancer Res. 25 (2005) 1139–1145. http://www.ncbi.nlm.nih.gov/pubmed/15868957.
[55] F.A. Al-Salmi, A.H. Alrohaimi, M. El Behery, W. Megahed, O.A. Abu Ali, F. G. Elsaid, E. Fayad, F.Z. Mohammed, A.T. Keshta, Anticancer studies of newly synthesized thiazole derivatives: synthesis, characterization, biological activity, and molecular docking, Crystals 13 (2023) 1546, https://doi.org/10.3390/cryst13111546.
[56] S. Tuzgen, H. Hanimoglu, T. Tanriverdi, T. Kacira, G.Z. Sanus, P. Atukeren, R. Dashti, K. Gumustas, B. Canbaz, M.Y. Kaynar, Relationship between DNA damage and total antioxidant capacity in patients with glioblastoma multiforme, Clin. Oncolo. 19 (19) (2007) 177–181, https://doi.org/10.1016/j.clon.2006.11.012.
[57] E. Lanez, Y. Bekkar, L. Bourougaa, M.L. Benamor, R. Bouraoui, O. Boudebia, A. Adiaka, K. Nesba, H. Chaoua, L. Bechki, T. Lanez, H. Alsaeedi, M. Bechelany, A. Barhoum, Antidiabetic potential of mentha piperita essential oil: GC-MS profiling, in vitro, in vivo and in silico analyses, J. Mol. Struct. 1351 (2025) 144239, https://doi.org/10.1016/j.molstruc.2025.144239.
[58] M.D. Mellaoui, K. Zaki, K. Abbiche, A. Imjjad, R. Boutiddar, A. Sbai, A. Jmiai, S. El Issami, A.M. Lamsabhi, H. Zejli, In silico anticancer activity of isoxazolidine and isoxazolines derivatives: DFT study, ADMET prediction, and molecular docking, J. Mol. Struct. 1308 (2024) 138330, https://doi.org/10.1016/j.molstruc.2024.138330.
[59] M.L. Ben Amor, E. Lanez, Y. Bekkar, A. Adaika, T. Lanez, K. Nesba, L. Bechki, Evaluation of ferrocenylmethylnucleobases derivatives interacting with DNA: insights from erlectrochemical, spectroscopic, DFT calculation, molecular docking and molecular dynamic simulations, Studia Universitatis Babes Bolyai Chemia 2025 (2025) 111–132, https://doi.org/10.24193/subbchem.2025.1.08.
[60] B. Samah, E. Lanez, M.L. Benamor, Y. Bekkar, N.N. Salah, L. Bourougaa, R. Bouraoui, S. Garzoli, T. Lanez, GC/MS analysis and computational evaluation of C. cinerea EO constituents for colorectal cancer: molecular docking, dynamics, and quantum chemical insights into cis-verbenyl acetate, Comput. Biol. Chem. 120 (2025) 108754, https://doi.org/10.1016/j.compbiolchem.2025.108754.
[61] A. Ailabouni, B. Prasad, Organic cation transporters 2: structure, regulation, functions, and clinical implications, Drug Metab. Dispos. 53 (2025) 100044, https://doi.org/10.1016/j.dmd.2025.100044.